AD-A128 899 INVESTIGATION FOR THE NOVEL FORMATION OF HIGH ENERGY PRODUCT FE COMPACTS(U) GENERAL ELECTRIC CORPORATE RESEARCH AND DEVELOPMENT SCHENECTA.. A E BERKOWITZ 1/1

UNCLASSIFIED MAY 83 83-SRD-022 N00014-81-C-0751 F/G 11/6 NL

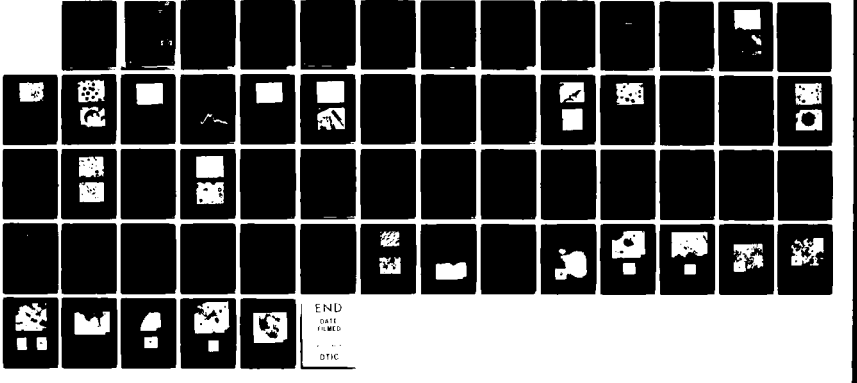

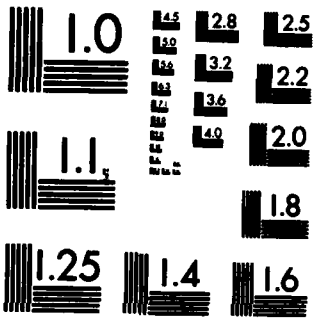

[redacted]

Final Report
Contract N00014-81-C-0751

Prepared for:

Department of the Navy
Office of Naval Research
Arlington, Virginia 22217

Prepared by:

A.E. Berkowitz
General Electric Company
Corporate Research and Development
Schenectady, New York 12301

May 1983

UNCLASSIFIED

SECURITY CLASSIFICATION OF THIS PAGE (When Data Entered)

REPORT DOCUMENTATION PAGE		READ INSTRUCTIONS BEFORE COMPLETING FORM
1. REPORT NUMBER	2. GOVT ACCESSION NO. AD-A128 899	3. RECIPIENT'S CATALOG NUMBER
4. TITLE (and Subtitle) Investigation for the Novel Formation of High Energy Product Fe Compacts		5. TYPE OF REPORT & PERIOD COVERED Final Report, 81 Sep 01 to 82 Aug 31
		6. PERFORMING ORG. REPORT NUMBER 83-SRD-022
7. AUTHOR(s) A.E. Berkowitz		8. CONTRACT OR GRANT NUMBER(s) Contract N00014-81-C-0751
9. PERFORMING ORGANIZATION NAME AND ADDRESS General Electric Company Corporate Research and Development Schenectady, NY 12301		10. PROGRAM ELEMENT, PROJECT, TASK AREA & WORK UNIT NUMBERS
11. CONTROLLING OFFICE NAME AND ADDRESS Department of the Navy Office of Naval Research Arlington, VA 22217		12. REPORT DATE May 1983
		13. NUMBER OF PAGES 55
14. MONITORING AGENCY NAME & ADDRESS (If different from Controlling Office)		15. SECURITY CLASS. (of this report)
		15a. DECLASSIFICATION/DOWNGRADING SCHEDULE

16. DISTRIBUTION STATEMENT (of this Report)

Approved for public release; distribution unlimited

17. DISTRIBUTION STATEMENT (of the abstract entered in Block 20, if different from Report)

18. SUPPLEMENTARY NOTES

19. KEY WORDS (Continue on reverse side if necessary and identify by block number)

permanent magnets, magnetic alloys, spark erosion, surface anisotropy

20. ABSTRACT (Continue on reverse side if necessary and identify by block number)

Two novel approaches were examined for the production of economical permanent magnets containing little or no critical materials. The first approach was to induce a strong surface anisotropy or spin pinning on Fe particles by coating them with suitable materials. Another aspect of this approach was to gain a deeper understanding of the mechanism of spin pinning. The principal positive result in this case was the establishment, by neutron diffraction, that spin pinning does occur on ferrite particles when

(continued on back)

DD FORM 1 JAN 73 1473 EDITION OF 1 NOV 65 IS OBSOLETE

UNCLASSIFIED

SECURITY CLASSIFICATION OF THIS PAGE (When Data Entered)

20. Abstract (Cont'd)

coated with oleic acid. The second approach was to prepare rapidly quenched precursor particles of various alloys and then anneal them to produce optimum magnetic properties. One result of this work was a demonstration of how different degrees of chemical short range order resulting from different quench rates yield different crystallization behavior, thus affording a measure of control over magnetic properties. Another important result of this phase was that very promising properties were produced in Mn-Al-C particles.

TABLE OF CONTENTS

--to be inserted in front of page 1--

INSERT FOR FINAL TECHNICAL REPORT - CONTRACT N00014-81-C-0751

FOREWORD

The investigations on alloys discussed in this report were carried out by A.E. Berkowitz in collaboration with J.L. Walter, J.M. Livingston, and I.S. Jacobs. A.F. Razzano made the magnetic measurements; C.R. Rodd made the optical micrographs; N. Lewis and C.W. Joyson made the scanning electron micrographs; E.F. Koch did the transmission electron microscopy; D.W. Marsh was responsible for the x-ray analysis.

The neutron diffraction and x-ray analyses of the organic coated ferrites was carried out by A.C. Nunes (University of Rhode Island) and C.F. Majkrzak (Brookhaven National Laboratories).

D.E. Polk was the contract supervisor for the Office of Naval Research.

INTRODUCTION

Two general approaches were examined to produce low cost, high energy product permanent magnets that do not use critical materials. The first was to establish a strong surface anisotropy on small Fe particles by means of appropriate coatings. This would be the metal particle analogue of the spin pinning observed in ferrite particles coated with various organic surfactants. The second approach was to prepare rapidly quenched particles of suitable compositions by the spark erosion technique. Control over the optimum structural heterogeneity of these particles for permanent magnet use could be obtained by choosing the initial particle size as well as by developing the desired crystallized state starting from a highly disordered structure. The progress in each of these areas will be described separately.

SURFACE ANISOTROPY/SPIN PINNING

Grinding Fe Particles with Surface Active Agents

Carbonyl Fe particles (~ 5 μm in diameter) were ground in an automatic apparatus using high density alumina mortars and pestles. The objective was to grind/smear the Fe particles to thin (~ 1 μm) platelets in the presence of surface active coating agents that would produce a strong surface anisotropy of the type observed on organic surfactant coated ferrite particles.[1,2] It was anticipated that grinding in the presence of the surface active agents would enhance the probability of strong bonding since freshly exposed, highly active particle surfaces would be continuously available. The surface active agents were chosen from three classes:

1. Oleic acid which was successful in producing spin pinning in ferrite particles[1,2]
2. Phosphate compounds. We used sodium metaphosphate $(NaPO_3)_6$ since Itoh et al.[3] had reported increased coercive force (H_c) on iron oxide particles treated with this compound. We also used several phosphate-based organic surfactants manufactured by General Analine and Film Company under the trade name GAFAC.
3. Since borides of Fe are often highly anisotropic, we used several compounds containing B.

Table 1 lists the milling conditions. The surface active agents were first dissolved in the carrier fluid to near saturation and then the grinding was carried out for the indicated times. The results were uniformly disappointing in that H_c never rose to more than 100 Oe at room temperature as compared to ~ 5 Oe in the premilled state. When the particles were examined in the optical microscope, it was evident that the grinding had not produced substantial changes in the average particle size. Thus it is not possible to state whether the observed increase in H_c results from an interaction due to the coatings or from milling stresses. Time limitations prevented examination of alternative methods for Fe particle size reduction with the presence of surface active agents.

Neutron and X-ray Diffraction Studies of Coated Ferrite Particles

The initial evidence for spin pinning on organic surfactant coated particles was provided by magnetic and Mössbauer measurements. To gain more insight into the mechanism responsible for the spin pinning, particularly with respect to surface spin

configurations, we initiated a collaboration with A.C. Nunes of Rhode Island University and C.F. Majkrzak of Brookhaven National Laboratories. $CoFe_2O_4$ particles (<100 Å in diameter), prepared by prolonged ball milling and coated with oleic acid,[2] were examined by x-ray and polarized neutron diffraction techniques. Line shape analyses were made on spectra taken on the as-prepared particles and after heating them for ten minutes in air at 300°C. The heating removed ~80% of the surfactant. The most significant result is that after the heating the average size of the coherently diffracting regions of the particles increased by ~45%. Since it is highly unlikely that the modest heating resulted in significant surface reconstitution, these results suggest that the bonding of the surfactant to the surface cations not only produces a strong local anisotropy, but also results in a highly strained surface which relaxes back to a normal lattice configuration when the surfactant is removed. These intriguing results are preliminary; the work is being continued. It does promise significant elucidation of some of the basic questions about the mechanism of spin pinning. A paper on this subject will be presented at the Third International Conference on Magnetic Fluids, June 1983, at the University of North Wales, Bangor, Wales. A draft copy of this paper is appended.

Table 1

Grinding Conditions for Fe Particles

Sample	Coating Agent	Carrier Liquid	Grinding Time(days)
1		dodecane	3
2	GAFAC RS-410	dodecane	8
3	GAFAC LO-529	dodecane	8
4	GAFAC RAM510	dodecane	21
5	$(NaPO_3)_6$	water	18
6	oleic acid	dodecane	20
7	O-Carborane	dodecane	15
8	decaborane	dodecane	60
9	lithium tetrahydidoborate	dodecane	64
10	sodium tetrahydidoborate	dodecane	64

CRYSTALLIZATION OF SPARK ERODED PARTICLES

The work in this area consisted of two parts. First, we conducted a study of the general implications of quenching rate on crystallization kinetics. Secondly, the bulk of the effort on the contract involved the preparation of rapidly quenched particles of a number of alloys by spark erosion and the characterization of the magnetic and structural properties of the alloys as a function of degree of crystallization.

Influence of Quenching Rate on Crystallization

The alloy $Fe_{75}Si_{15}B_{10}$ (atom%) was chosen for this investigation because we have studied this system rather extensively in both the crystalline[4,5] and amorphous[6–8] states. Chill cast ribbon and particles spark eroded in dodecane were prepared. The particle diameters ranged from ~0.5 to 30 μm. All samples were amorphous as indicated by their x-ray diffraction spectra. It had been previously established[7] that the quench rate for the spark-eroded particles was higher than that of the ribbon. From magnetic[6] and energy dispersive x-ray[8] studies, we concluded that the spark eroded particles had less chemical short range order (CSRO) than did the ribbon. The object of the present study was to determine whether the differences in quench rate and CSRO influenced the crystallization kinetics and/or phases appearing. A paper on this work has been accepted for publication by *Mat. Sci. Eng.* and is appended to this report, the principal results are summarized in that paper as follows.

Crystallization characteristics of both forms of the amorphous alloy were measured by differential scanning calorimetry, x-ray diffraction, and transmission electron microscopy. The crystallization temperature, T_x, of the largest particles was higher than that of the ribbon. Both T_x and the heat of crystallization increased with decreasing particle size. The DSC thermograms also showed marked differences from ribbon to particles and with decreasing particle size.

The first crystals to form on heating the ribbon were the stable phases alpha iron and Fe_3Si. At higher temperatures, Fe_2B and $Fe_3(Si,B)$ crystals appeared along with the Fe_3Si crystals as the final crystallization product. On the other hand, the first crystals to form in the powder were the metastable b.c. tetragonal Fe_3B. At higher temperatures, Fe_3Si, $Fe_3(Si,B)$ and Fe_2B crystals formed. Previous work has shown that the particles are more chemically disordered than the ribbon, leading to the conclusion that there is a greater probability for the iron atoms in the particles to have more boron atoms as neighbors compared with the ribbon. These Fe-B "clusters" in the particles act as nuclei for formation and growth of the nonequilibrium Fe_3B crystals in the particles. Subsequent transformation of the Fe_3B at higher temperatures produces the final crystallization products of Fe_2B, Fe_3Si, and $Fe_3(Si,B)$.

Since significant differences in intermediate crystallization products result from different quench rates, it is important to examine how these differences are reflected in the magnetic properties. This work is well underway and will be reported on completion.

Spark-Eroded Particles For Permanent Magnet Alloys

Preparation

All of the particles of permanent magnet alloys were prepared in the apparatus sketched in Figure 1. The cylindrical glass container is 10 cm in diameter. Electrodes of the alloy, typically 5 to 7 cm long are mounted on a screen in the container through which the spark-eroded particles could fall to the bottom. The space between the electrodes is filled with pieces of the alloy ~2 to 6 mm in diameter. The electrodes were connected to a relaxatron oscillator (R-C tank circuit) charged to ~200 V with a rectifier. Capacitor sizes up to 25 μF may be selected. When the gaps between electrodes and particles are appropriate, the capacitor discharges. The container is vibrated to keep the charge particles from welding, and to provide the correct discharge gaps. When required (e.g., for cryogenic dielectric fluids), the glass container is placed in a dewar with a cooling liquid.

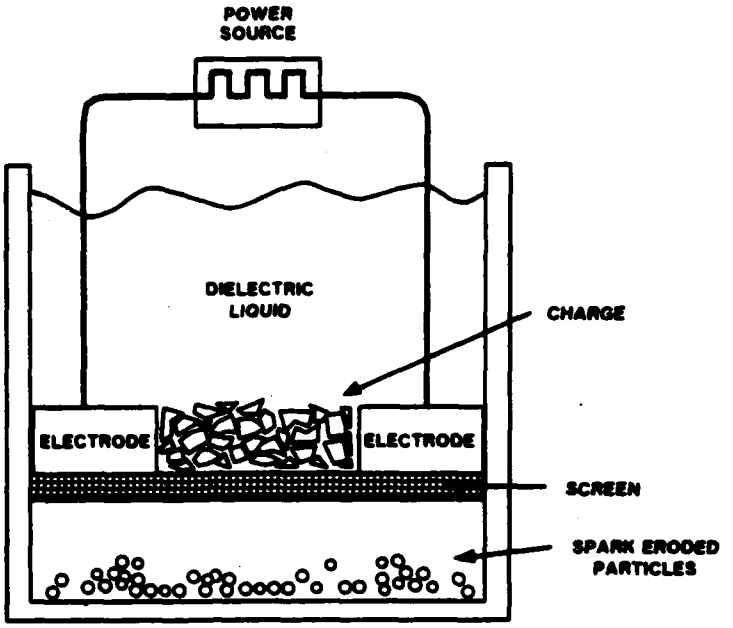

Figure 1. Sketch of apparatus used to prepare permanent magnet alloys by spark erosion.

Two general points about spark erosion[7] may be noted here. First, the existence of a spark implies a dielectric breakdown of the fluid. If the dielectric fluid is organic, the breakdown products include C, O, H, and some polymeric material. Reactive electrodes or charge material may thus form carbides, oxides, etc. This occurs when, for example, the electrodes are Fe. If reactive elements are sufficiently alloyed, there is no carbide formation. The $Fe_{75}Si_{15}B_{10}$ spark-eroded particles do not contain any C. Liquid Ar or, in some cases, liquid N_2 can be used as dielectrics to avoid carbide or oxide formation. These liquids, of course, are much more volatile than hydrocarbons such as dodecane. There are several effects of the lower heat capacity and boiling points of cryogenic liquids. The quench rate is lowered since most of the cooling is in a gaseous environment. Also, if an alloy is composed of elements with greatly different vapor pressures, there is more likelihood of preferential loss of the more volatile component in a cryogenic than in an organic dielectric. The second general point is that spark-eroded particles are produced by highly localized heating of the electrodes and charge. Therefore if the starting materials are coarse-grained multiphase alloys, the spark-eroded particles that are smaller than the grain size will have compositions that deviate from the nominal alloy composition. Both of these effects were manifest during the course of this work.

When the particles were prepared using a cryogenic liquid dielectric, an Ar gas cover was maintained during the run. At the end of such a run the cryogenic liquid was permitted to boil off under the Ar cover. With organic dielectrics, the product was washed in acetone with ultrasonic agitation and permitted to settle overnight. Particles >0.5 μm settled out, were collected and rewashed twice. Dried particles were served in an Allen-Bradley Sonic Sifter. Particles were sized into ranges <10, 10-20, 20-30, 30-38 μm.

$Fe_{73.8}B_{16.2}La_5Tb_5$ and $Fe_{74}B_{16}MM_{10}$ Particles Prepared by Spark Erosion

The investigation of $Fe_{73.8}B_{16.2}La_5Tb_5$ was stimulated by the work of Koon et al.[9,10] who reported maximum H_c values of ~10 kOe when amorphous ribbons of this composition were crystallized at ~ 650°C. They reported that optimum properties were associated with the presence of fine grained Fe_3B and R_2Fe_{23} as the principal phases. Overaging developed coarser grained Fe_2B and α-Fe with drastically decreased H_c. An Fe/B ratio at least as great as 73.8/16.2 was also required.

Chill cast slabs, 8 × 13 × 1.3 cm, were prepared from which electrodes and charge material were obtained. Figure 2 shows optical micrographs of this slab. A very coarse grained structure is evident in a fine grained eutetic matrix. An attempt was made to homogenize the structure by annealing at 955°C for 66 hr in Ar. Figure 3 shows a micrograph of the resulting structure. There is little change from the structure in Figure 2. As discussed above, such a coarse-grained structure for the electrodes and charge makes it unlikely that the small spark-eroded particles will have the nominal composition of the starting material.

Table 2 lists the preparation conditions and magnetic properties for spark-eroded particles of this electrode composition. Particles were prepared in dodecane as well as in N_2-cooled liquid Ar. We consider first the particles prepared in dodecane. X-ray spectra showed a mixture of amorphous and crystalline phases. The crystalline phases were α-Fe and Fe_2B, the two phases associated with deteriorated magnetic properties.[10] Figure 4 shows optical micrographs of sectioned 20-30 μm particles and scanning electron micrographs (SEM) of particles in the same size range. The optical micrographs are consistent with the x-ray data. There are completely amorphous particles (white), completely crystalline particles (dark), and particles that are mixtures of amorphous and crystalline phases (mottled). Thus the coarse-grained structure of the electrode and charge prevented the production of a significant percentage of particles with the nominal starting composition and an amorphous structure. The magnetic properties of these particles in Table 1 reflect this situation. Both the <10 and 30-38 μm particles show low H_c values in the as-prepared condition that do not change significantly after anneals in the optimum region.[9] These low values probably arise because the equilibrium α-Fe and Fe_2B phases are magnetically soft and they are already present in the as-prepared particles. The initial presence of a small amount of amorphous material is indicated by the fact that the hysteresis loops of the annealed samples remain open, even at 25 kOe.

The x-ray data for the particles spark eroded in N_2-cooled Ar using $Fe_{73.8}B_{16.2}La_5Tb_5$ electrodes and charge were similar to the product from the dodecane run: a mixed amorphous and crystalline structure with α-Fe and Fe_2B as the major crystalline phases. A wider range of particle sizes was examined than for the dodecane case, as listed in Table 2. The same low H_c values were found for the same reasons as in the dodecane case. The open hysteresis loops at high fields were even more prevalent in this case.

Charge material was prepared with the composition $Fe_{74}B_{16}MM^*_{10}$ where MM* signifies Ce-free mischmetal. We were, of course, interested in the possibility that the cheaper mischmetal might be a useful substitute for the pure rare earths. Figure 5 shows an optical micrograph of the charge material. A fine-grained eutectic structure is evident in contrast to the coarse-grained structures in Figures 2 and 3 for the material containing Tb_5La_5. Since the chill cast slab was extremely brittle, it could only be used for charge material. We used electrolytic Fe electrodes for the spark erosion.

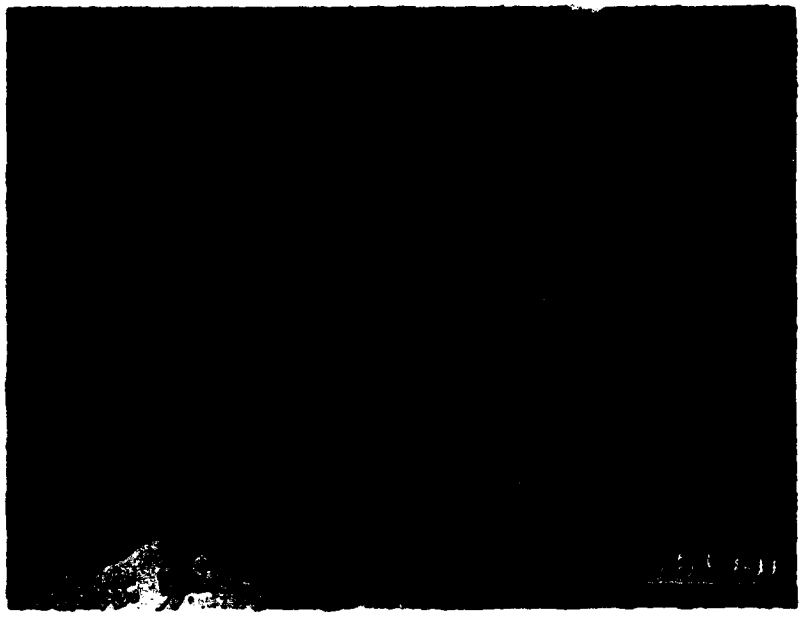

(a)

(b)

Figure 2. Optical micrographs of polished sections of chill-cast alloy $Fe_{73.8}B_{16.2}Tb_5La_5$.

Table 2

Preparation Conditions and Magnetic Properties of $Fe_{73.8}B_{16.2}La_5Tb_5$ and $Fe_{74}B_{16}MM_{10}$ Spark Eroded Particles

Composition	Dielectric	Heat Treatment (°C/hrs)	Diam. (μm)	σ, 25kOe (emu/gm)	H_c (Oe)
$Fe_{73.8}B_{16.2}Tb_5La_5$	dodecane	as-prepared	<10	106	120
		652/16	<10	125	170
		677/16	<10	131	160
		as-prepared	30-38	112	~0
		652/16	30-38	132	110
		677/16	30-38	132	120
$Fe_{73.8}B_{16.2}Tb_5La_5$	N_2-cooled Ar	as-prepared	38-75	88	130
		655/16	38-75	106	180
		as-prepared	30-38	87	80
		655/16	30-38	120	95
		as-prepared	20-30	83	20
		550/1	20-30	118	20
		655/16	20-30	128	75
		as-prepared	10-20	88	20
		279/1	10-20	91	20
		315/1.5	10-20	82	10
		550/1	10-20	115	20
		655/16	10-20	129	80
		as-prepared	<10	81	10
		550/1	<10	112	20
		550/1	<10	130	40
$Fe_{74}B_{16}MM_{10}$	Ar	as-prepared	<10	96	10
		350/1	<10	99	20
		450/1	<10	122	30
		530/1	<10	134	30
		680/16	<10	144	10
		as-prepared	30-38	117	85
		680/16	30-38	145	85

Figure 3. Optical micrograph of polished section of chill-cast alloy $Fe_{73.8}$ $B_{16.2}Tb_5La_5$ after annealing at 955°C for 66 hr in Ar.

Figure 6a shows the x-ray spectrum of 10-20 μm particles spark eroded in dodecane. The sample is almost completely crystalline. The major phase is α-Fe; the minor phase is isostructural with PrC_2. Thus, in spite of the fine-grained structure, spark erosion in dodecane produced a crystalline product because of the reaction of the mischmetal with the C which was present as a result of the breakdown of the organic dielectric.

Figure 6b shows the x-ray spectrum of 10-20 μm particles spark eroded in liquid Ar. These particles are mostly amorphous with one crystalline peak occurring at 2.02 Å which is probably α-Fe. Thus, when reaction of C with mischmetal is not a problem, the fine-grained structure of the $Fe_{74}B_{16}$ MM_{10} charge results in amorphous particles. The Fe line evidently arises from erosion of the Fe electrodes. Figure 7 is an SEM of these particles. Although most of the particles are spheroidal, there are many particles with irregular shapes. This is characteristic of particles spark eroded in cryogenic liquids. The magnetic properties of the <10 and 30-38 μm particles are listed in Table 2. Neither the as-prepared nor the annealed sample show interesting properties, although open hysteresis loops up to 25 kOe were very evident. Since the mischmetal is principally La, it appears that the Tb in the compostion reported by Koon et al. is certainly a necessity for useful hysteresis properties.

The results for the Fe-B-Re alloys investigated may be summarized as:

1. The coarse-grained structure of the electrodes and charge material did not produce a product of amorphous particles which are essential for the development of the fine-grained Fe_3B and Fe_{23} Re_6 phases responsible for high energy product.
2. Substituting mischmetal for La and Tb produced fine-grained charge material and amorphous particles, but the lack of Tb prevented the devlopment of useful permanent magnets.

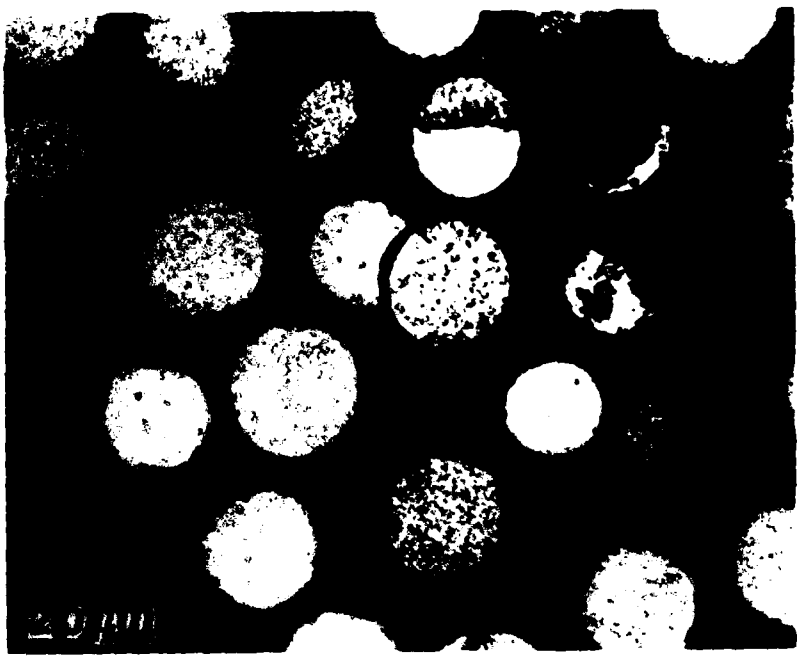

(a)

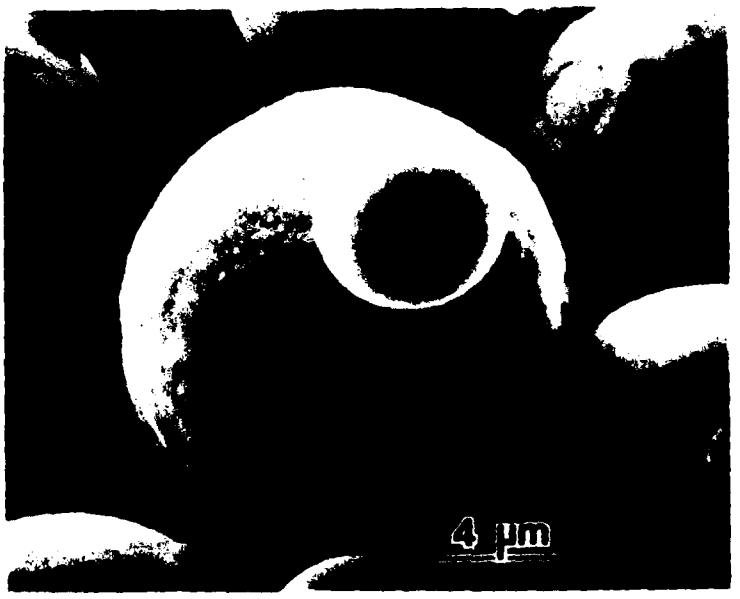

(b)

Figure 4. **(a) Optical micrographs of sections and (b) scanning electron micrographs of 20-30 μm particles sparks eroded in dodecane with $Fe_{73.8}$ $B_{16.2}Tb_5La_5$ electrodes and charge.**

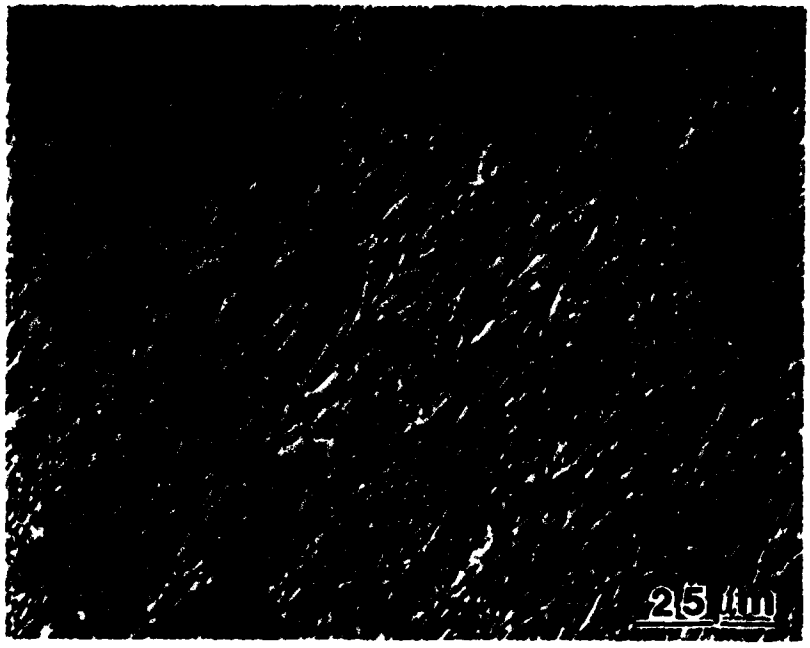

Figure 5. Optical micrograph of section of $Fe_{74}B_{16}$ MM* charge material.

$Fe_{60}Nd_{40}$ and $Fe_{60}Pr_{40}$ Particles Prepared by Spark Erosion

The work of Croat[11] on $Fe_{60}Re_{40}$ (atom%) alloys has shown that when they are prepared by melt spinning at intermediate rates, some rather high H_c values (~8 kOe for Pr, Nd) are obtained. We prepared chill cast slabs of $Fe_{60}Nd_{40}$, $Fe_{60}Pr_{40}$, and $Fe_{60}MM_{40}$. Micrographs of Nd and MM alloys are shown in Figure 8. Both structures are very coarse. In this case, the MM structure is coarser than the $Fe_{60}Nd_{40}$ structure. The $Fe_{60}Pr_{40}$ structure was the same as that of the $Fe_{60}Pr_{40}$. The brittle nature of the alloys precluded preparation of electrodes; therefore, Fe electrodes were used with alloy charge. N_2-cooled liquid Ar was used as the dielectric, both to avoid the formation of RE-carbides and to reduce the quench rate from that obtained with dodecane.

X-ray spectra of the $Fe_{60}Nd_{40}$ and $Fe_{69}Pr_{40}$ spark-eroded particles showed a structure that was mostly amorphous, with a number of crystalline peaks. Many of these crystalline peaks had 2θ values that were similar to those reported by Croat[10] for $Fe_{60}Nd_{40}$. The lack of complete agreement was due to the coarse-grained charge material and the use of Fe electrodes. Table 3 lists come magnetic properties for these particles. H_c values increased with decreasing particle size and did not improve with moderate aging. Maximum values of ~1000 Oe were achieved, much less than the ~8 kOe reported by Croat for $Fe_{60}Nd_{40}$ and $Fe_{60}Pr_{40}$. As in the case with the $Fe_{73.8}B_{16.2}Tb_5La_5$ system, a major problem was the coarse-grained charge material which precluded the production of particles with the proper composition.

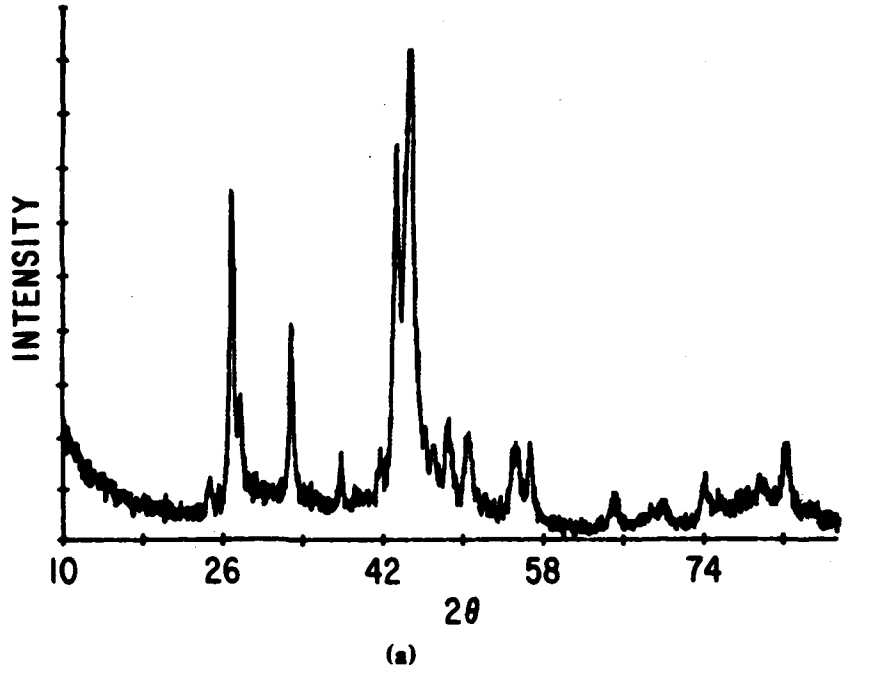

(a)

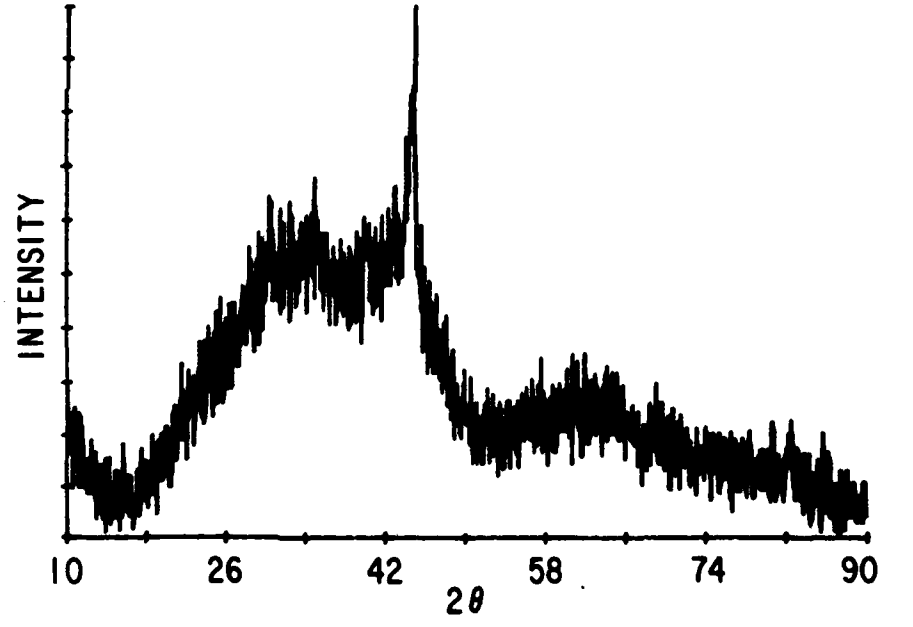

(b)

Figure 6. X-ray diffraction spectra of 10-20 μm particles produced from $Fe_{74}B_{16}MM^{*}$ charge material and Fe electrodes by spark erosion in (a) dodecane and (b) liquid Ar.

Figure 7. Scanning electron micrograph of 10-20 μm particles spark eroded in liquid Ar using an $Fe_{74}B_{16}MM^*$ charge and Fe electrodes.

Table 3

Preparation Conditions and Magnetic Properties of $Fe_{60}Nd_{40}$ and $Fe_{60}Pr_{40}$ Spark Eroded Particles

Composition	Dielectric	Heat Treatment (°C/hr)	Diam (μm)	σ, 25kOe (emu/gm)	H_c (Oe) (Oe)
$Fe_{60}Pr_{40}$ Fe electrodes	N_2-cooled Ar	as-prepared	<10	54	1060
		as-prepared	10-20	59	820
		as-prepared	20-30	60	760
		as-prepared	30-38	56	600
$Fe_{60}Nd_{40}$ Fe electrodes	N_2-cooled Ar	as-prepared	40	51	860
		+ 170/1	40	53	740
		+ 300/1	40	53	550
		as-prepared	10-20	59	860
		as-prepared	20-30	59	860
		as-prepared	30-38	63	670

(a)

(b)

Figure 8. Optical micrograph of section of (a) $Fe_{60}Nd_{40}$ and (b) $Fe_{60}MM_{40}$ charge material.

Mn-Al-C ALLOYS

The origin of coercivity in these magnets is the high crystal anisotropy of the τ-phase, the only ferromagnetic phase in the Mn-Al system. Of approximate composition $Mn_{70}Al_{30}$ (wt%), the τ-phase has the face-centered-tetragonal CuAu(I) structure. This phase has a Curie temperature above 350°C, a saturation magnetization of 7 to 8 kG, and an anisotropy field of 40-60 kOe.

The τ-phase is metastable, the usual phase transformation sequence on cooling, or on quenching followed by heating, being $\epsilon \rightarrow \epsilon' \rightarrow \tau \rightarrow \gamma + \beta$. The high-temperature equilibrium h.c.p. phase ϵ orders along one of three close-packed directions to form ϵ', which then can shear in one of two directions to form τ. Thus this transformation sequence can produce six different orientation variants of τ from a single crystal of ϵ. At longer annealing times, τ decomposes eutectoidally into the low-temperature equilibrium phases, $\gamma + \beta$.

The τ-phase can dissolve up to 0.5 wt% C, which greatly slows down the eutectoid decomposition and allows thermomechanical processing of the τ-phase. The dissolved C appears to have little effect on magnetization and anisotropy field, but does lower the Curie temperature to about 300°C. Carbon contents slightly beyond the solubility limit usually produce some Mn_3AlC, which apparently does not harm magnetic properties and has even been claimed to be beneficial. Nevertheless, to keep sufficient C in solution, and to maintain subsequent workability, cooling rates must be sufficient to avoid substantial carbide precipitation during cooling. Higher C and Al contents can lead to formation of Al_4C_3. This carbide is very deleterious, since it reacts with moisture at room temperature, leading to severe cracking and sometimes complete disintegration of the alloy.

Workers from Philips reported[12] coercivities up to 6 kOe in MnAl powders produced by grinding. They also noted that grinding produced a decrease in magnetization, presumably resulting from disordering introduced by plastic deformation. Aging the powder increased the moment but decreased the coercivity. They also found that swaging a bar of MnAl produced a partly-aligned magnet with B_r = 4.3 kG , H_c = 4.6 kOe, and $(BH)_{max}$ = 3.5 MGOe.

Workers at Matsushita[13] later extended the Philips work by making additions of carbon and studying a great variety of compositions and heat treatments. By solution treating at about 900°C, quenching at 300°C/min or higher, and then aging between 480 and 650°C, isotropic magnets were produced with energy products up to 1.7 MGOe. By subsequent extruding at 700°C, followed by aging at 700°C, anisotropic magnets could be produced with B_r = 5.8 kG, H_c = 3.2 kOe, $(BH)_{max}$ = 6.3 MGOe. Willems[14] has reported on isotropic magnets prepared from powders produced by melt extraction. For magnets with 0.5 wt% C, he obtained B_r = 3.4 kG, H_c = 1660 Oe, and $(BH)_{max}$ = 1.5 (MGO).

We have examined a variety of approaches for this system. Spark-eroded particles have been prepared for $Mn_{69.5}Al_{30}Co_{0.5}$ (wt%) electrodes and charge in dodecane and liquid Ar. We have used reactive spark erosion to introduce the C by spark eroding $Mn_{70}Al_{30}$ electrodes and charge in dodecane and ethyl alcohol. The composition $Mn_{71.5}Al_{28}C_{0.5}$ has also been examined. The electrode and charge material in each case was annealed at 1000°C for 3 hr in Ar to insure homogeneity. The general objective was to prepare particles that were initially in the high temperature hexagonal ϵ-phase and then anneal them to develop the optimum magnetic τ-phase.

$Mn_{69.5}Al_{30.0}C_{0.5}$ in Dodecane

For this composition, ribbon was prepared by chill casting in order to serve as a reference point, particularly with respect to magnetization. Table 4 summarizes the annealing conditions and the resulting magnetic properties; all anneals on these and the spark eroded samples were carried out in purified N_2. The values in Table 4 are similar to those reported by Willems[13] for particles of the same composition prepared by melt extraction. Willems' H_c values were about 1600 Oe.

Spark erosion of $Mn_{69.5}Al_{30.0}C_{0.5}$ in dodecane was the test system for the Mn-Al-C particles, and a large number of runs were made. Some typical run conditions and magnetic data are shown in Table 5. As-prepared, the x-ray spectra of all particles showed only the high temperature hexagonal ϵ-phase. Figure 9 is an SEM of $<10\mu$m as-prepared particles. The surface features on the generally spherical larger particles may be a thin polymer coating due to pyrolysis of the dodecane. C-analysis showed a much higher C-content than the initial 0.5 wt%. For example, the 20-30 μm particles contained 2.5 wt% C, m the smaller particles even more. X-ray analysis of annealed particles showed the magnetic τ phase as the major phase, minor amounts of the equilibrium phases, and traces of Mn_3AlC. Chemical analysis of the particles showed that the Mn concentration was 2.5 wt% (20-30 μm) and 3.5 wt% (<10 μm) lower in the spark-eroded particles than in the original charge. Apparently, the higher vapor pressure of the Mn as compared to Al was responsible for this behavior.

As shown in Table 5, we annealed the 20-30 μm particles for 1 hr at temperatures between 650 and 700°C to find the temperature producing the highest moment. This temperature was 675°C; samples of all sizes were then annealed for 1 hr at 675°C. From Table 5, we see that σ decreases and H_c increases with decreasing particle size. Since higher C and decreasing Mn- content were also associated with decreasing diameter, the particle size dependence of deviations from nominal composition can certainly account for the moment behavior. We are currently analyzing the dependence of the microstructure on particle size to gain a clearer understanding of the moment and coercivity behavior. We note the 20-30 μm particles show a BH_{max} of 1.2 MGOe.

$Mn_{69.5}Al_{30.0}C_{0.5}$ in Liquid Ar

In order to avoid carbide production, particles were prepared by spark erosion in liquid Ar for $Mn_{69.5}Al_{30.0}C_{0.5}$ electrodes and charge. Two power settings (i.e. condensor sizes) were used: the normal high setting ($\sim$25 μF) and the medium setting ($\sim$12 μF). The results were not encouraging. We seemed to have traded one set of problems for another. The lower boiling point and specific heat of the Ar seemed to encourage dissociation of the alloy and the vapor sheath from the boiling Ar produced slower cooling. X-ray spectra of as-prepared particles showed the presence of significant amounts of phases other than the deserved hexagonal ϵ-phase, particularly for the smaller particle sizes. Lower power was beneficial in this regard. Apparently there was less preferential vaporization of the Mn with respect to Al. Figure 10 is an SEM of the <10 μm particles produced at medium power. Powdery "debris" is visible in addition to the spherical particles. Presumably this "debris" consists of very fine particles which would not be collected from a dodecane run, since they would be enmeshed in the polymer. With the Ar, these very fine, likely non-stoichiometric particles are present. Figure 11 shows an optical micrograph of 20-30 μm particles also prepared at medium power. The multiphase nature is evident. The low moments in

Table 6 are consistent with these structural problems. However, it is evident that lower power sparks are beneficial in this case, i.e., higher σ values are attained.

Table 4

Annealing Conditions and Magnetic Properties of Chill Cast Ribbon, $Mn_{69.5}Al_{30.0}C_{0.5}$ (wt %)

Annealing Temperature(°C)	Anneal Time(hr)	σ,25kOe (emu/gm)	H_c (Oe)
450	0.25	82.0	1375
450	1	104.6	1360
450	2	102.5	1330
450	20	101.6	1345
500	0.25	94.6	1345
500	1	101.4	1310
500	4	102.2	1310
500	20	104.0	1375
550	0.25	102.1	1310
550	1	102.6	1310
550	4	104.5	1310

Table 5

Annealing Conditions and Magnetic Properties of Particles Spark Eroded in Dodecane with $Mn_{69.5}Al_{30.0}C_{0.5}$ (wt %) Electrodes and Charge

Diameter (μm)	Temperature (°C)	Time (hr)	σ,25kOe (emu/gm)	H_c (Oe)
20-30	650	1	58.6	
	662	1	67.2	
	675	1	70.0	
	687	1	66.2	
	700	1	48.8	
<10	675	1	63.6	3130
10-20	675	1	66.2	3120
20-30	675	1	70.0	3005
30-38	675	1	71.3	2895
38-75	675	1	72.3	2775

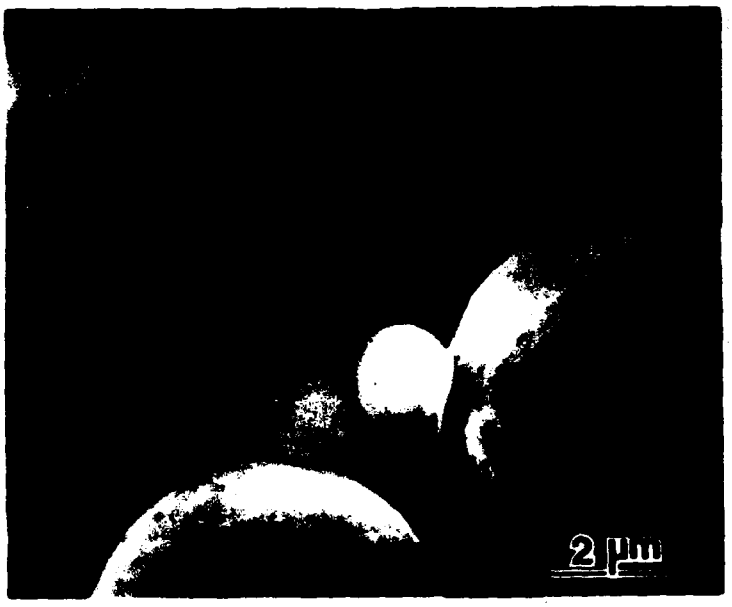

Figure 9. Scanning electron micrograph of $< 10\ \mu m$ particles spark eroded in dodecane for $Mn_{69.5}Al_{30.0}C_{0.5}$ (wt%) electrodes and charge.

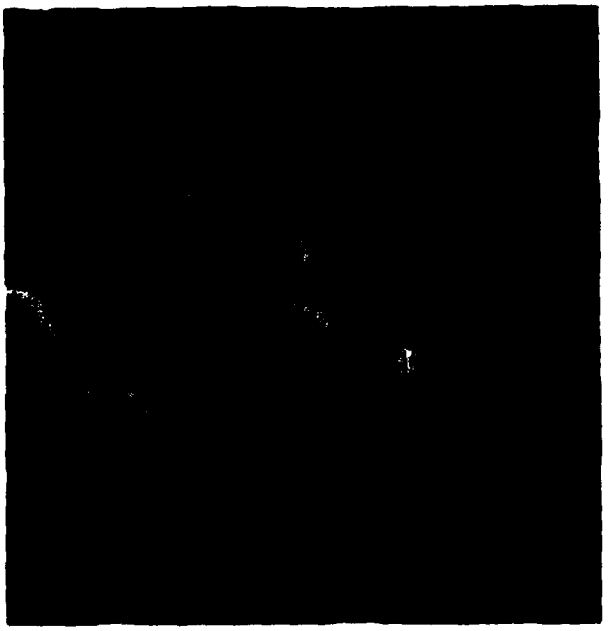

Figure 10. Scanning electron micrograph of $< 10\ \mu m$ particles spark eroded in liquid Ar at medium power from $Mn_{69.5}Al_{30.0}C_{0.5}$ (wt%) electrodes and charge.

Figure 11. Optical micrograph of sections of 20-30 μm particles spark eroded in liquid Ar at medium power from $Mn_{69.5}Al_{30.0}C_{0.5}$ (wt%) electrodes and charge.

Table 6

Annealing Conditions and Magnetic Properties of Particles Spark Eroded in Liquid Ar with $Mn_{69.5}Al_{30.0}C_{0.5}$ Electrodes and Charge

Diameter (μm)	Power	Temperature (°C)	Time (hr)	σ,25kOe (emu/gm)	H_c (Oe)
< 10	High	600	0.5	8.9	2370
	High	600	1	12.4	2500
	High	600	16	16.0	2655
10-20	High	600	0.5	20.4	2215
	High	600	1	30.8	2290
	High	600	16	34.2	2420
20-30	High	600	0.5	57.5	
			15	69.2	2090
	Medium				
< 10	Medium	600	15	28.5	2690
10-20	Medium	600	15	50.5	2330
20-30	Medium	600	15	71.9	1975

$Mn_{70}Al_{30}$ in Dodecane

It seemed logical to provide the C by reactive spark erosion of $Mn_{70}Al_{30}$ in dodecane. These samples were analyzed for C, and indeed the C-content varied monotonically from 3.36 wt% C for <10 μm particles to 2.04 wt% C for 30-38 μm particles. The <10 μm sample also showed $\sim$1 wt% less Mn than the 20-30 μm sample. X-ray spectra of these particles indicated only the presence of the high-temperature hexagonal ϵ-phase; there was no indication of any carbides in the as-prepared particles. After annealing, however, there were possible traces of Mn_3AlC. A possible explanation of the lack of x-ray indication of carbides in the as-prepared samples is that most of the C present was in a pyrolyzed surface layer which reacted with the particles on annealing. Figure 12 shows the fine structure of the as-prepared particles of the two size extremes.

The dependence of σ and H_c on annealing time and temperature is shown in Table 7. Moments are higher in the optimal region than with the previously discussed preparation methods. Considering the 575°C anneal, the <10 μm sample annealed for 1 hr and the 20-30 μm sample annealed for the same time have BH_{max} values of 1.2 and 1.4 MGOe, respectively. The hysteresis loop of the latter sample is shown in Figure13. Two features may be noted. The large high field slope results from the >40 kOe anisotropy field in these materials. It is probable that alignment while sintering these particles into billets would significantly increase the energy product, as reported by Itoh et al.[3] This is also suggested by the fact that the loop is open at the maxium applied field, i.e. there are some extremely hard particles in this sample.

$Mn_{70}Al_{30}$ in Ethyl Alcohol

In order to examine the effects of reducing C content, particles were spark eroded in ethyl alcohol from $Mn_{70}Al_{30}$ electrodes and charge. Chemical analysis showed that the C was about 50% of that found in particles prepared in dodecane. X-ray analysis showed that both the <10 and 20-30 μm as-prepared particles contained the ϵ-phase with a trace of the equilibrium Al_8Mn_5 phase; there was no x-ray indication of carbide. After annealing the particles, the x-ray spectra showed the magnetic τ phase with traces of the equilibrium phases and no evidence for carbides. Figure 14 shows SEMs of <10 and 20-30 μm particles as-prepared. We note that some of the 20-30 μm particles are composed of clusters of smaller particles. Such particles are not characteristic of spark erosion in dodecane and may be a consequence of the lower boiling point of the ethyl alcohol and the reduced polymer production, i.e. the smaller particles are not as likely to be enmeshed in the polymer and therefore can collect in a lightly sintered cluster.

Table 8 shows some magnetic data after annealing. Samples were given successive anneals for the total times indicated. The particles were immobilized in paraffin only after the last anneal. Thus only this H_c is indicated. We note that lower temperatures seem to produce optimum properties than is the case with particles prepared in dodecane. This may be a consequence of lower C. Together with the lack of x-ray evidence for carbides, this behavior may suggest again that the C found by chemical analyses is mostly a pyrolyzed surface layer. The lower moments and higher H_c for the smaller particles is again evident in Table 8. The H_c of the <10 μm particles annealed 22 hr at 500°C is 3840 Oe. The hysteresis loop of these particles is shown in Figure 15. The very high slope and open loop at the highest fields indicate the potential

Table 7

Annealing Conditions and Magnetic Properties of Particles Spark Eroded in Dodecane with $Mn_{70}Al_{30}$ (wt %) Electrodes and Charge

Diameter (μm)	Temperature (°C)	Time (hr)	σ ,25kOe (emu/gm)	H_c (Oe)
<10	500	0.25	62.1	2785
		0.5	66.5	2925
		1	70.4	3065
		2	71.5	3240
20-30	500	0.25	70.0	2845
		0.5	74.9	3005
		1	77.3	3130
		2	76.1	3275
<10	575	0.25	74.4	3370
		0.5	74.6	3555
		1	72.9	3555
		2	70.2	3570
20-30	575	0.25	78.7	3240
		0.5	80.7	3240
		1	80.6	3225
		2	74.5	3200
<10	600	0.25	70.6	3480
<10	625	0.25	73.2	3480
<10	650	0.25	72.0	3415
<10	675	0.25	74.6	3320
		0.5	69.2	3320
		1	69.7	3240
		2	62.9	3250
10-20	675	0.25	76.6	3130
		0.5	73.0	3145
		1	70.6	3085
		2	66.9	3085
20-30	675	0.25	72.2	2875
		0.5	76.3	2925
		1	72.5	2965
		2	69.0	2855
30-38	675	0.25	74.0	2815
		0.5	75.3	2665
		1	78.3	2690
		2	70.9	2765
38-75	675	0.25	76.5	2610
		0.5	76.3	2660
		1	77.1	2640
		2	73.1	261

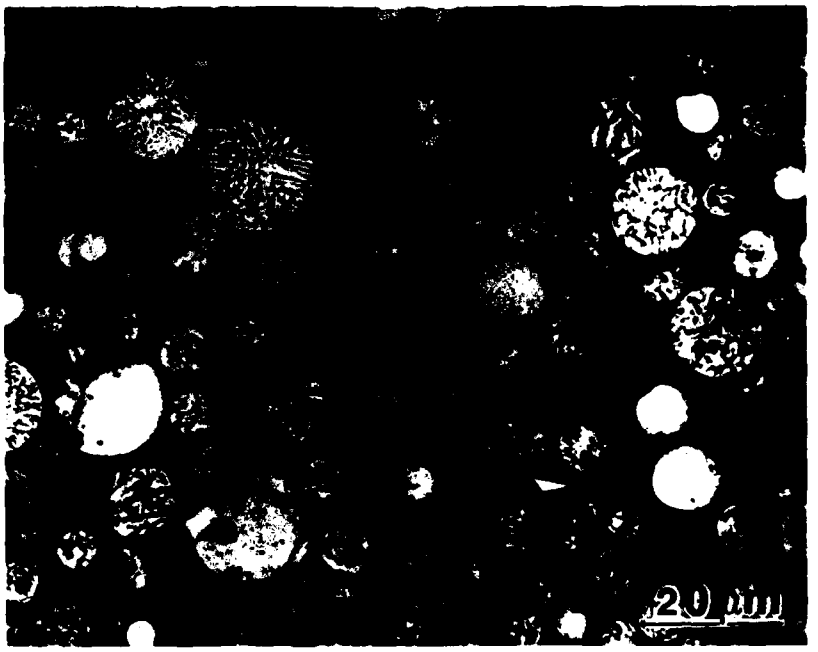

(a)

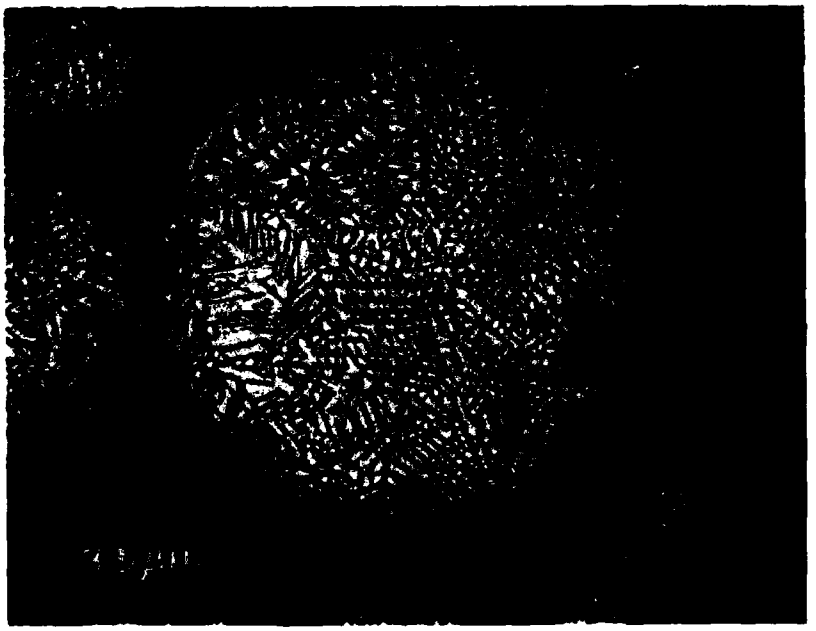

(b)

Figure 12. Optical micrographs of sectioned particles prepared by spark erosion in dodecane of $Mn_{70}Al_{30}$ (wt %) electrodes and charge; (a) <10 μm, (b) 38-75 μm.

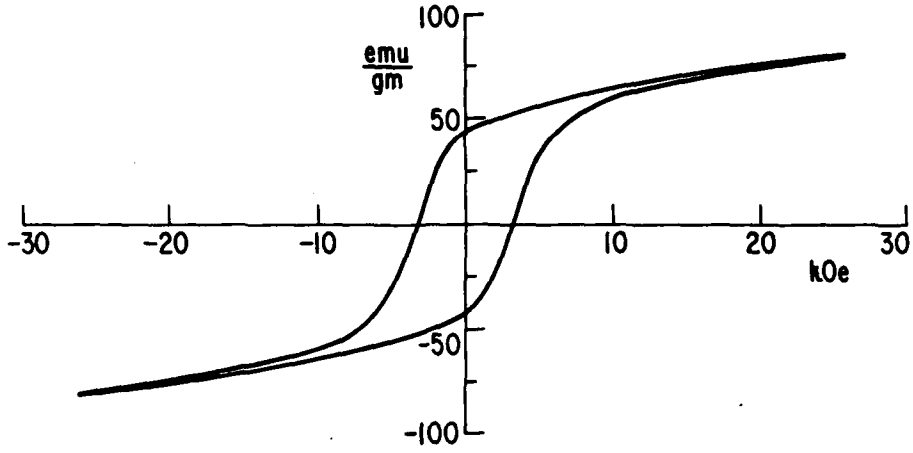

Figure 13. Hysteresis loop of 20-30 μm diameter particles spark eroded in dodecane using $Mn_{70}Al_{30}$ (wt%) electrodes and charge after annealing 1 hr at 575°C.

for much higher energy product. Figure 16 shows sections of <10 and 20 - 30 μm particles annealed 16 hr at 500°C. There is considerable difficulty in resolving the features in the smaller particles due to problems of preparing sections of such small particles. However, one gets the impression of considerably smaller crystallite sizes in the <10 μm particles. We hope to resolve this question with transmission electron microscopy. If indeed there are much smaller crystallites in the <10 μm, this might explain both the lower moment and higher H_c. The moment might be lower because of the larger volume of disordered alloy on the surfaces of the grains of the <10 μm particles. The higher H_c may simply result from a more nearly single domain size for the crystallites in the smaller particles. The question is basic to deciding on optimum preparation conditions.

$Mn_{71.5}$ $Al_8C_{0.5}$ in Dodecane

Particles were spark eroded in dodecane using electrodes and charge with a higher Mn content to counter the preferential vaporization of Mn. The composition examined was $Mn_{71.5}Al_{28.0}$ $C_{0.5}$ (wt%). Table 9 lists some results for various anneals. These samples were annealed successively at the indicated temperatures and only after the last anneal was the sample immobilized for a reliable H_c measurement. We note that the highest H_c values for both the <10 and 20 - 30 μm samples encountered in the Mn-Al-C system are those for 4 hr at 550°C for this sample. The examination of this system is in a very preliminary stage. However, it does appear that there is some merit in adjusting composition.

Summary of Mn-Al-C Results

Although this work is not completed, it is clear that spark eroded particles are very promising materials for producing sintered compacts. The energy products are in the same range as the best isotropic magnets previously reported. It is clear that optimization of composition and dielectric used will bring further improvement. Hot pressing and/or hot swaging this material is the next step.

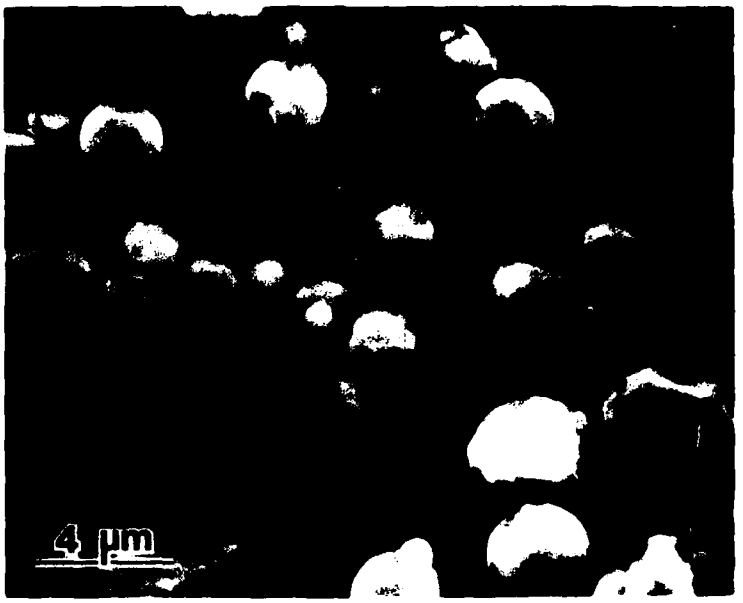

(a)

(b)

Figure 14. Scanning electron micrographs of particles prepared by spark erosion in ethyl alcohol using $Mn_{70}Al_{30}$ (wt%) electrodes and charge; (a) <10 μm, (b) 20-30 μm.

Table 8

Annealing Conditions and Magnetic Properties of Particles Spark Eroded in Ethyl Alcohol From $Mn_{70}Al_{30}$ (wt %) Electrodes and Charge

Diameter (μm)	Temperature (°C)	Time (hr)	σ, 25kOe (emu/gm)	H_c (Oe)
<10	500	0.25	54.1	
		1	60.3	
		2	60.5	
		6	62.6	
		22	53.9	3840
20-30	500	0.25	59.3	
		1	71.7	
		2	74.6	
		6	76.9	
		22	79.1	2690
<10	525	0.25	59.4	
		0.5	61.4	
		1	62.5	
		2	60.3	3400
20-30	525	0.25	70.2	
		0.5	75.3	
		1	76.4	
		2	78.4	2420

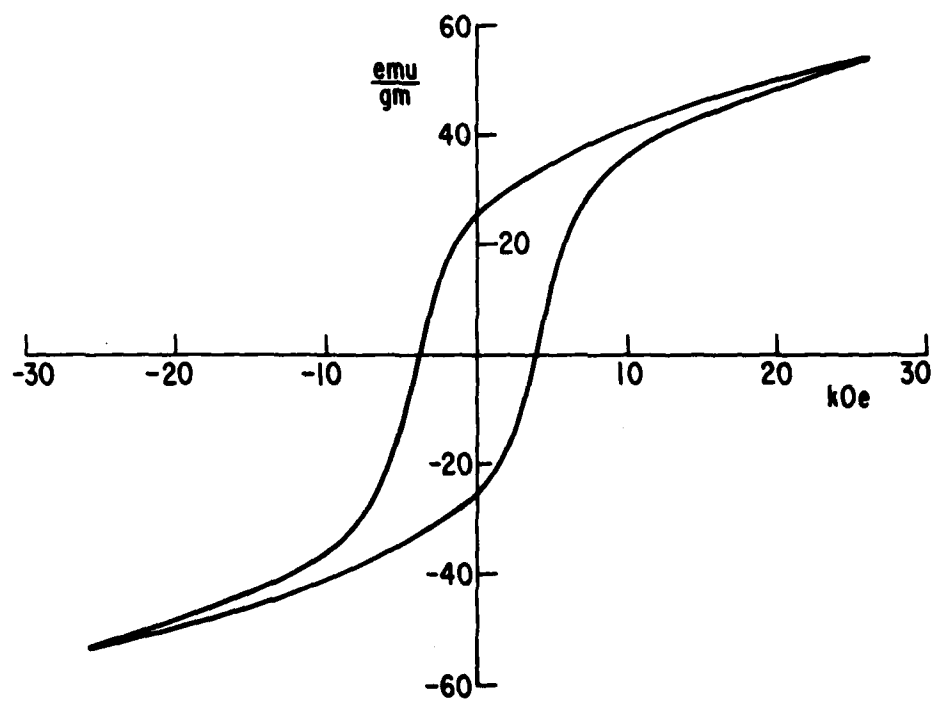

Figure 15. Hysteresis loop of <10 μm particles spark eroded in ethyl alcohol from $Mn_{70}Al_{30}$ (wt%) electrodes and charge. Particles annealed 22 hr at 500°C in N_2.

(a)

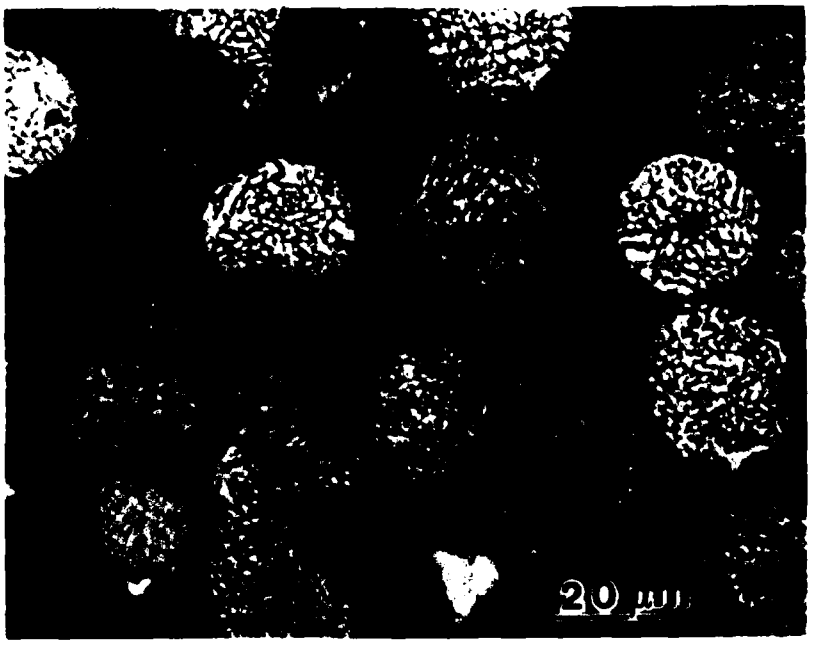

(b)

Figure 16. *Optical micrographs of sectioned particles prepared by spark erosion in ethyl alcohol using $Mn_{70}Al_{30}$ (wt%) electrodes and charge. Particles annealed 16 hr at 500°C in N_2; (a) <10 μm, (b) 20-30 μm.*

Table 9

Annealing Conditions and Magnetic Properties for Particles Spark Eroded in Dodecane Using $Mn_{71.5}Al_{28.0}C_{0.5}$ (wt %) Electrodes and Charge

Diameter (μm)	Temperature (°C)	Time (hr)	σ ,25kOe (emu/gm)	H_c (Oe)
< 10	450	0.25	37.2	
		1	53.0	
		2	57.1	
		4	61.8	
		20	57.5	2325
20-30	450	0.25	15.3	
		1	51.9	
		2	68.0	
		4	75.4	
		20	72.7	3255
< 10	500	0.25	58.1	
		1	59.5	
		4	58.8	
		20	50.5	
20-30	500	0.25	68.4	
		1	77.5	
		4	77.3	
		20	68.3	
< 10	550	0.25	60.6	
		1	65.1	
		4	53.1	3860
20-30	550	0.25	73.6	
		1	72.6	
		4	69.6	3635

PUBLICATIONS

1. "Polarized Neutron Study of Magnetization Density Distribution Within a $CoFe_2O_4$ Colloidal Particle," A.C. Nunes, C.F. Majkrzak, and A.E. Berkowitz, to be published in *J. Magn. Mag. Mat.*, draft provided as Appendix A.
2. "Crystallization of Amorphous $Fe_{75}Si_{15}B_{10}$ Ribbon and Powder" J.L. Walter, A.E. Berkowitz and E.F. Koch, to be published in *Mat. Sci. Eng.*, provided as Appendix B.

We expect to publish a paper on the dependence of hysteresis properties on the different crystallization stages and kinetics resulting from different quenching rates in spark eroded and chill cast ribbon of composition $Fe_{75}Si_{15}B_{10}$.

A paper on spark eroded Mn-Al-C particles will be published.

REFERENCES

1. A.E. Berkowitz, J.A. Lahut, I.S. Jacobs, L.M. Levinson, and D.W. Forester, *Phys. Rev. Lett. 34,* 594 (1975).
2. A.E. Berkowitz, J.A. Lahut, C.E. VanBuren, *IEEE Trans. Magn. MAG-16,* 184 (1980).
3. F. Itoh, M. Satou, and Y. Yamazaki, *IEEE Trans. Magn. MAG-13,* 1385 (1977).
4. A.E. Berkowitz, J.E. Livingston, B.D. Nathan, and J.L. Walter, *J. Appl. Phys. 50,* 1754 (1979).
5. J.D. Livingston, A.E. Berkowitz, and J.L. Walter, *IEEE Trans. Magn. MAG-15,* 1295 (1979).
6. A.E. Berkowitz, J.L. Walter, and K.F. Wall, *Phys. Rev. Lett. 46,* 1484 (1981).
7. A.E. Berkowitz and J.L. Walter, *Mat. Sci. Eng. 55,* 275 (1982).
8. S. Aur, T. Egami, A.E. Berkowitz, and J.L. Walter, *Phys. Rev. B 26,* 6355 (1982).
9. N.C. Koon and B.N. Das, *Appl. Phys. Lett. 39,* 840 (1981).
10. N.C. Koon, B.N. Das, and J.A. Geohegan, *IEEE Trans. Magn. MAG-18,* 1448 (1982).
11. J.J. Croat, *IEEE Trans. Magn. MAG-18,* 1442 (1982).
12. A.J.J. Koch, P. Hokkeling, M.G. vd Steeg, and K.J. DeVos, *J.Appl. Phys. 31,* 755 (1960).
13. T.Ohtani, N. Kato, S. Kojima, K. Kojima, Y. Sakamoto, I. Konno, M. Tsukahara, and T. Kubo, *IEEE Trans. Magn. MAG-13,* 1328 (1977).
14. R.H. Willems, *IEEE Trans. Magn. MAG-16,* 1059 (1980).

APPENDIX A

Appendix A

Submitted to the
THIRD INTERNATIONAL CONFERENCE
ON
MAGNETIC FLUIDS

28-30 June 1983

POLARIZED NEUTRON STUDY OF THE MAGNETIZATION DENSITY DISTRIBUTION WITHIN A $CoFe_2O_4$ COLLOIDAL PARTICLE* (MAGNETIZATION DENSITY IN A COLLOIDAL $CoFe_2O_4$ CRYSTALLITE)

A.C. Nunes, C.F. Majkrzak, A.E. Berkowitz†

KEY WORDS: Neutron, $CoFe_2O_4$, particle

* Work supported by (ACN) NSF Grant DMR-8024662; (CFM) DOE Contract DE-ACO2-76CH00016; (AEB) ONRL Contract N00014-81-C-0751

† A.C. Nunes, Physics Dept., University of Rhode Island, Kingston, RI 02881, USA.
C.F. Majkrzak, Physics Dept. Brookhaven National Laboratory, Upton, NY 11973, USA.
A.E. Berkowitz, General Electric Corporate Research and Development, Schenectady, NY 12301, USA.

ABSTRACT

Magnetization and Mössbauer data suggest that a magnetically anomalous region exists within finely divided $CoFe_2O_4$ particles when coated with oleic acid [1]. We have undertaken an x-ray and polarized neutron powder diffraction study of these samples with and without the surfactant coating in an attempt to locate and characterize this anomalous zone. The shape of neutron scans of the (4,0,0) reflection are independent of polarization, indicating that the reflecting crystallites are uniformly magnetized. Magnetization calculated from the peak flipping ratio is characteristic of uncoated rather than coated particles in both cases. Scan widths of both x-rays and neutrons are narrower for the sample from which the chemisorbed surfactant has been largely removed, indicating an increase in the size of the coherent lattice of a crystallite. These observations are consistent with the existence of a highly strained surface layer roughly 10 Å thick characterized by pinned spins associated with the presence of oleic acid, which relaxes to a more normal lattice structure upon boiling off the surfactant.

I. INTRODUCTION

We wish to present preliminary findings of an investigation into the magnetization density distribution within very finely divided $CoFe_2O_4$ particles (diameter $\sim$100 Å) employing x-ray and polarized neutron powder diffraction line shape analysis. Berkowitz et al. [1] report magnetization and Mössbauer data taken on these samples which suggest that a magnetically anomalous region exists within the particles when coated with a chemisobed surfactant, oleic acid. This anomalous region, presumed to exist at the ferrite-surfactant interface, may comprise nearly half of the ferrite volume of the particle and is characterized by pinning of the magnetically ordered spins. These "pinned spins" are not polarized in an externally applied field of 207 kOe. In the present work, we investigate the internal magnetization density distribution and the crystallite size of the ferrite particles with the surfactant intact and after having driven off much of the surfactant by heating. Through these investigations, we gain further insight into the atomic events which give rise to the observed magnetic behavior.

Two questions are addressed here:

- Is the magnetically anomalous behavior localized at the particle-surfactant interface or is the entire volume of the particle somehow affected?
- To what extent is the crystal structure of the ferrite modified by the presence of the surfactant?

II. METHOD

We are employing polarized neutron powder line shape analysis to determine the radial distribution of the magnetization density within a tiny magnetic particle. To our knowledge, this is the first such study and so deserves some elucidation.

Consider an unstrained spherical crystal of radius R. It can be shown [2] that the intensity scattered at an angle $\delta\theta$ from a Bragg reflection (scattering angle = $2\theta_o$) will be proportional to

$$I(q) = (F(h,k,l)G(R,q))^2 \qquad (1)$$

where $F(h,k,l)$ is the structure factor associated with the Bragg reflection identified by the Miller indices h,k, and l. $G(R,q)$ is the spherical Bessel function given by

$$G(R,q) = 4\pi R^3 \left[\frac{\sin Rq}{(Rq)^3} - \frac{\cos Rq}{(Rq)^2} \right] \tag{2}$$

and

$$q = \frac{4\pi(\sin(\theta_o + \delta\theta) - \sin\theta_o)}{\lambda} \tag{3}$$

$I(q)$ is approximately a Gaussian whose width Δq is inversely proportional to R. Thus from Δq (the powder line width corrected for instrumental broadening), one can determine the size of the crystallite in Å from

$$R = 3.652/\Delta q \tag{4}$$

where Δq is the full width at half maximum of I(q) expressed in $Å^{-1}$.

If the particles are ferromagnetic and polarized perpendicular to the scattering plane, and the incident neutrons are also polarized parallel (+) or antiparallel (-) to the sample magnetization, the structure factor becomes the sum of magnetic $\pm F_M$ and nuclear F_N parts [3]

$$F(h,k,l) = F_N(h,k,l) \pm F_M(h,k,l). \tag{5}$$

If the magnetization is evenly distributed throughout the crystal, only the magnitude, not the width of I(q) will vary with the neutron polarization state (sign of F_M). If the magnetization is restricted to a spherical core, leaving a nonmagnetic spherical shell of thickness ΔR, Eq. (1) becomes

$$I(q) = \left[(F_N \pm F_M) G(R - \Delta R, q) + F_N(G(R,q) - G(R - \Delta R, q)) \right]^2 \tag{6}$$

which simplifies to

$$I(q) = (F_N G(R,q) \pm F_M G(R - \Delta R, q))^2 \tag{7}$$

This is also true if the outer layer is paramagnetic or composed of randomly oriented pinned spins, in which case there will be magnetic scattering from the shell, but it will be incoherent and will not contribute to the Bragg intensity. Note that now not only the magnitude but also the shape of $I(q)$ is dependent on the sign of the neutron polarization. If R is 50 Å and ΔR is 10 Å, using nuclear and magnetic structure factors determined by Prince [4], one finds that the width of the (4,0,0) reflection of $CoFe_2O_4$ (for which $|F_M| \simeq |F_N|$) should vary by more than 10% with a change in neutron polarization. Also the integral flipping ratio, given by

$$R(h,k,l) = \frac{\int I_+(q)\,dq}{\int I_-(q)\,dq} \tag{8}$$

will be approximately 6, as opposed to $R_o(4,0,0) = 97$ for a uniformly magnetized sample. The fraction specific magnetization of the particle (total magnetization relative to the saturation value) is found from

$$M = \frac{F_N}{F_M}\left[\frac{R_o + 1 \pm 2\sqrt{R}}{R-1}\right] \tag{9}$$

Eq. (9) has two solutions, and one must choose the more physically sensible.

It should be noted that if one replaces the structure factor with a scattering density and performs the experiment at $(h,k,l) = (0,0,0)$, all formulae remain otherwise unchanged; however, the experiment is often called "small angle" rather than powder scattering. Magnetic small angle scattering experiments have been reported on nickel [5] and cobalt [6]; however, interparticle interference terms can be very important, especially if chaining or particle agglomeration is significant [7,8] and cannot be ignored. Interparticle interference is usually unimportant in Bragg scattering, as the very stringent lattice coherence requirement between two particles for such interference in a powder reflection renders the probability of such events extremely small.

Additional complications are introduced by the fact that the particles are neither perfectly spherical nor monodispersed. Electron micrographs [1] show particle images which are irregular but approximately spherical. This has the effect of altering the constant in equation (4) by at most a few percent (see particle shape dependence of the Scherrer constant, Table X.1, James [2]). Electron micrographs of similarly prepared particles also show the particle size to be log normally distributed [9]

$$P(R) = N_o e^{-1/2\left[\frac{\ln R - \ln R_o}{\ln \sigma}\right]^2} \tag{10}$$

with approximate parameters R $\sim$ 50 Å, ln $\sigma \approx 0.2$. To include this quantity, equation (7) becomes

$$I(q) = \int_{R=0}^{\infty} (F_N G(R) \pm FMG(R-\Delta R))^2 P(R)\,dR \tag{11}$$

The effect of properly including $P(R)$ is to change the constant of Eq. (4) from 3.65 to 2.71. The expected sample flipping ratio is increased (to $\sim$ 10); however, the magnitude of the change in Δq with neutron polarization is little altered.

Therefore, from measurements $I_+(q)$ and $I_-(q)$ for certain powder reflections, one should be able to determine sample magnetization (as a fraction of the saturation value, Eq. 9) and, from the polarization-dependent widths Δq_+ and Δq_-, determine R and ΔR of the particle.

III. SAMPLE PREPARATION

Samples were prepared by prolonged grinding in a ball mill in kerosene and oleic acid, followed by centrifugation and washing as described in Reference 1. Chemical analysis reveals contaminants from the mill, and mill balls are present [1]. In seeking evidence of these contaminants in x-ray powder patterns of two samples, one $CoFe_2O_4$ and the other MgO (both prepared in the same way), we found none. We conclude that the contaminants do not contribute significantly to the observed Bragg peaks, but rather to the background scatter.

After grinding and centrifuging at 17 kG's for 20 minutes, the suspended material remaining was dried and washed with methylene chloride, leaving particles coated with one to two monolayers of oleic acid [1]. A portion of this was then heated in air for 10 minutes at 300 °C, which removed more than 80% of the remaining surfactant.

IV. SCATTERING EXPERIMENTS

Polarized neutron scattering experiments were performed at the High Flux Beam Reactor at Brookhaven National Laboratory. The monochromator was a bent pyrolytic graphite crystal. Beam polarization was provided after the sample with a Heusler alloy crystal. Beam polarization was characterized by a flipping ratio of ± 1. The sample was mounted in a flat aluminum sample holder in a 4.5 kOe field perpendicular to the scattering plane. No depolarization of the beam transmitted through the sample could be detected.

X-ray powder data was taken on a $\theta-2\theta$ diffractometer at the University of Rhode Island. The results of both neutron and x-ray scans of the (4,0,0) reflection of $CoFe_2O_4$ are summarized in Table 1. Peak widths Δq have been corrected for instrument resolution.

Table 1

SUMMARY OF EXPERIMENTAL RESULTS OF POLARIZED NEUTRON AND X-RAY STUDY OF THE (4,0,0) BRAGG REFLECTION OF $CoFe_2O_4$ COLLOIDAL PARTICLES IN A MAGNETIC FIELD OF 4.5 kOe

Sample	Neutron-Sample Polarization	Neutron Scan q Width Δq_N ($Å^{-1}$)	Flipping Ratio R	% Magnetization M	X-Ray q Width Δq_x ($Å^{-1}$)	Particle Radius $R_o=2.71/\Delta q_x$ (Å)
$CoFe_2O_4$ +	↑ ↑	0.08 ±0.003	3.4 ±0.3	(37 ±1)%	0.092 ±0.003	29 ±1
Oleic Acid	↑ ↓	0.085 ±0.003				
$CoFe_2O_4$	↑ ↑	0.069 ±0.001	3.8 ±0.1	(39 ±1)%	0.065 ±0.001	42 ±0.6
After Heating	↑ ↓	0.070 ±0.002				

V. DISCUSSION

There are three striking features of these data. First, the percent magnetization of the ferrite derived from the flipping ratio is unchanged by boiling off most of the surfactant, and its value is approximately that derived from magnetization experiments on the *uncoated* particles [1]. Second, the neutron scan widths are, within statistics, polarization-independent, indicating that the magnetization is uniformly distributed throughout the coherently scattering part of the crystallite. Third, the size of the coherently scattering region of the particle R_o is significantly increased by boiling off most of the surfactant. As it seems unlikely that annealing $CoFe_2O_4$ at 300°C for ten minutes can result in significant melting and recrystallization, we tentatively interpret this apparent "particle growth" as a relaxing of a seriously strained surface back to normal ferrite lattice positions with the removal of the surfactant.

These observations and those of reference 1 are consistent with a model in which the chemisorption of oleic acid on the surface of $CoFe_2O_4$ causes spin pinning at the surface and simultaneously distorts the surface region of the ferrite such that those molecules can no longer participate in the Bragg scattering from the crystallite. This surface layer is approximately 10 Å (~2 molecules) thick. The percent magnetization of the inner unstrained region of the particle is lower than that measured for bulk $CoFe_2O_4$, and while it is consistent with magnetization measurements on very small particles, this indicates that even when uncoated, no region of these tiny particles is truly "bulk like" in character.

In these respects, these results are similar to recently reported NMR studies of chemisorption on tiny platinum particles [10], leading to the following questions:

- How large must a particle be to be "bulk like"?
- How do material characteristics depend upon particle size?
- Is the surface of a large particle similar to that of a very small one, or is the curvature of the surface as important (or more important than) the simple density discontinuity?

The need for more work, both theoretical and experimental, is recognized.

REFERENCES

1. A.E. Berkowitz, J.A. Lahut and C.E. Van Buren, *IEE Trans. MAG-16* (1980), 184.
2. R.W. James, *The Optical Principles of the Diffraction of X-rays*, Cornell University Press, Ithaca, NY (1965), 528-540.
3. G.E. Bacon, L, *Neutron Diffraction*, 2nd ed., Oxford, (1962), 179.
4. E. Prince, *Phys. Rev. 102*, No. 3, (1956), 674.
5. M. Sato and H. Hirakawa, *J. Phys. Soc. Japan 39*, No. 6, (1975), 1467.
6. D.J. Cebula, S.W. Charles, and J. Popplewell, *Colloid Polym. Sci. 25*0, (1981), 395.
7. D.A. Krueger, *IEEE Trans. MAG-16*, (1980), 251.
8. J.B. Hayter and R. Pynn, *Phys. Rev. Lett. 49*, No. 15, (1982), 1103.
9. G.F. Neilson, *J. Appl. Cryst. 6*, (1973), 386.
10. H.E. Rhodes, P.K. Wang, H.T. Stokes, C.P. Slichter and J.H. Sinfelt, *Phys. Rev. B26* No. 7 (1982), 3559.

APPENDIX B

GENERAL ELECTRIC

General Electric Company
Corporate Research and Development
Schenectady, New York 12345

TECHNICAL INFORMATION SERIES

AUTHOR
Walter, JL
Berkowitz, AE*
Koch, EF†

SUBJECT
amorphous metals, crystallization

NO.
82CRD319

DATE
December 1982

GE CLASS
1

NO. PAGES
18

TITLE
Crystallization of Amorphous $Fe_{75}Si_{15}B_{10}$ Ribbon and Powder

ORIGINATING COMPONENT
Metallurgy Laboratory

CORPORATE RESEARCH AND DEVELOPMENT
SCHENECTADY, N.Y.

SUMMARY

Amorphous ribbon and powder of the alloy $Fe_{75}Si_{15}B_{10}$ were prepared by chill casting and by spark erosion, respectively. Samples of ribbon and powder were heated to temperatures corresponding to some fraction of crystallization in the differential scanning calorimeter (DSC). Other samples were heated isothermally in vacuo or in purified nitrogen to cause grain growth. Crystallization temperatures, T_x, measured by differential scanning calorimetry, were higher for the larger particles than for the ribbon and T_x and the heat of crystallization increased with decreasing particle size. The first crystals to form in the ribbon, as determined by transmission electron microscopy, were the stable phases alpha Fe and Fe_3Si. At higher temperatures, Fe_2B and $Fe_3(Si,B)$ crystals appeared along with the Fe_3Si as the final crystallization product. The first crystals to form in the spark eroded powder were the metastable b.c. tetragonal Fe_3B. At higher temperatures, Fe_3Si, $Fe_3(Si,B)$, and Fe_2B crystals formed. It was concluded that Fe-B "clusters" in the more chemically disordered particles act as nuclei for formation of the Fe_3B crystals. The more chemically ordered ribbon forms only the equilibrium or stable phases on crystallization.

KEY WORDS
amorphous metals, amorphous ribbon, amorphous powder, spark erosion, annealing, crystallization

INFORMATION PREPARED FOR _____

Additional Hard or Microfiche Copies Available from

Technical Information Exchange
Bldg. 5 Room 321, Schenectady, N.Y. 12345

Crystallization of Amorphous $Fe_{75}Si_{15}B_{10}$ Ribbon and Powder

J.L. Walter, A.E. Berkowitz, and E.F. Koch

1. INTRODUCTION

The alloy $Fe_{75}Si_{15}B_{10}$ (atom percent) has been formed as amorphous ribbon by chill casting and as amorphous powder by spark erosion in organic dielectrics.[1-4] The spontaneous magnetization, σ_o, and the Curie temperature, T_c, were lower in particles of similar dimensions as the ribbon and both decreased with decreasing particle size. Mössbauer spectra taken at 295 K and 77 K showed a reduction in peak and mean hyperfine fields and an increase in line width from the ribbon through the smaller particles. These results were interpreted to mean that the chemical short range order (CSRO) of the ribbon was greater than that of the particles and that the CSRO decreased with decreasing particle size.[3] It was concluded that the reduction in CSRO was the result of an increase in metalloid concentration around some iron sites in the amorphous matrix.[3] Recent measurements of the radial distribution function of both ribbon and particles by the energy dispersive X-ray diffraction technique are also consistent with decreased compositional short range order in the particles compared with the ribbon.*

The crystallization temperature, as measured by differential scanning calorimetry (DSC), increased from ribbon to particles and increased with decreasing particle size.[4] This difference in crystallization temperature, together with differences in the number of crystallization events in DSC,[4] indicated significant differences in the mechanism of crystallization which could arise from the structural differences in these amorphous $Fe_{75}Si_{15}B_{10}$ alloys. For this reason, we have examined samples of ribbon and powder at various stages of crystallization using X-ray diffraction and transmission electron microscopy.

2. EXPERIMENTAL PROCEDURE

The starting material for ribbon and powder preparation was a 1.2 cm thick slab melted and cast under argon into a copper chill mold. The constituents were 99.9% Fe, 99.8% B, and Si with 1 ppb impurities. The ribbons were cast on a 15 cm diameter copper drum at surface speeds of 30 and 43 m/s.[5] Ribbon thicknesses were 17.5 and 27 μm, respectively, and they were 1-2 mm wide.

The powders were produced by spark erosion which consists essentially of maintaining a repetitive spark discharge between two electrodes immersed in a dielectric fluid as discussed in References 2 and 4. The dielectric fluid was dodecane ($CH_3(CH_2)_{10}CH_3$). The spark discharge caused small regions of the electrodes to be heated rapidly above the melting temperature to produce small molten droplets or vaporized regions which were ejected into the dielectric to be rapidly quenched. The particles were generally less than 40 microns in diameter. Size fractions in the range 0.5 microns to 38 microns were prepared by sieving. All ribbon and powder samples were examined by X-ray diffraction initially to be certain that they were amorphous. Samples of ribbon and powders were annealed in two ways. The long term anneals were performed by sealing the sample in glass or quartz tubes which were evacuated, backfilled with purified nitrogen, and sealed. Other samples were annealed in vacuo. All of these samples were annealed isothermally. Other samples of approximately 5 mg weight were heated in a Perkin-Elmer DSC at 40°C/min. to determine the crystallization temperatures and characteristics. New samples were then heated in the DSC to a predetermined temperature corresponding to some fraction of complete crystallization. These annealed samples were also examined by X-ray diffraction.

Magnetic properties of all samples were measured with a vibrating sample magnetometer (VSM) in fields up to 25 KOe. An atmosphere of nitrogen was maintained in the instrument during measurements above room temperature. The usual heating rate was about 7°C/min. Curie temperatures, T_c, of the amorphous phase and any crystalline phases formed on heating were determined by temperature sweeps in the VSM in 50 Oe applied field. T_c data provided information concerning the crystalline phases formed on annealing.

Both ribbon and powder samples were examined by transmission electron microscopy (TEM) in the as-formed state and after partial and complete crystallization. The technique for preparation of the powder samples for TEM is described elsewhere.[6]

* Measurements and interpretations by S. Aur and T. Egami of the University of Pennsylvania. To be published in "Physical Review."

Manuscript received November 19, 1982.

3. EXPERIMENTAL RESULTS

Figure 1 shows a scanning electron micrograph of particles of $Fe_{75}Si_{15}B_{10}$ formed by spark erosion in dodecane. They are generally smooth and spherical with no surface structure or coating. Etched sections of unscreened particles, Figure 2, show no sign of crystals except for the largest particles, those in excess of about 50 microns in diameter. An X-ray diffractometer trace is shown in Figure 3a for particles less than 38 microns diameter and in Figure 3b for 27 μm thick ribbon. The diffractometer pattern for both showed two broad maxima. Table I lists the d-values for various powder and ribbon samples. These d-values yield an atom-to-atom distance of about 2.47 A which is related to Fe-Fe pairs. In the size range up to 38 μm the particles are completely amorphous. The cast ribbon is similarly amorphous.

3.1 Long Term Anneals Below the Crystallization Temperature

Samples of ribbon and particles were annealed at 633 K and 648 K for 27 and 21 days, respectively, in purified nitrogen. Examination of the annealed samples by transmission electron microscopy (TEM) showed no variations in microstructure except for the ribbon sample heated at 648 K. In this sample were a very few alpha-iron crystals similar to those in the hypoeutectic Fe-B alloys heated to the first stage of crystallization.[7] These crystals existed only near the edge of the ribbon. The d-values (listed in Table I) are sharply reduced for the ribbon by the 21-day anneal at 648 K while the d-values for the particles, initially the same as the ribbon, did not change on annealing. Figure 4 shows a transmission electron micrograph and the selected area diffraction pattern of a particle of 20-30 micron powder heated for 21 days at 648 K. There was no evidence, either in ribbons or particles, of the formation of microcrystals of supersaturated solid solutions observed by others[8-10] in alloys of similar composition annealed at similar temperatures for similar lengths of time.

Table I

d-VALUES OF AMPOPHOUS PHASE OF RIBBONS AND POWDERS

Anneal	Ribbon	Particles 10-20μ	Particles 20-30 μ
None	2.03		2.04
	1.22		1.21
	1.03		1.03
633K-27 days	2.02		
	1.22		
	1.02		
648K-21 days	1.95		2.04
	1.16		1.20
	0.99		1.04
Beginnining Cryst.	2.00	2.04	2.04
	1.20	1.22	1.21
	1.03	1.05	
50% Crystallization			2.04
			1.21

Mössbauer spectra were obtained at 295 K and fitted with a distribution of hyperfine fields, p(H), determined by the Fourier series method of Window.[11] The data for H_{mean} from as-prepared ribbon and powder and after the 21-day anneal at 648 K are given in Table II.

Table II

MÖSSBAUER DATA FROM AMORPHOUS $Fe_{75}Si_{15}B_{10}$ RIBBON AND PARTICLES

Sample	H_{mean} (295K) kOe As-prepared	648K-21 days	% change
Ribbon	245	243	-0.8
20-30 μm	205	223	+9.0
10-20 μm	186	202	+9.0

3.2 Differential Scanning Calorimetry

Figure 5 shows examples of DSC thermograms for the ribbon and various size fractions of the powders. The heating rate was 40°C/min. There are two differences between the ribbon and the powder. First, the thermogram of the ribbon exhibits two crystallization events as is indicated by the two peaks. There is also a third broad exothermic feature at higher temperatures. Kemeny et al[12] have reported two exothermic peaks for amorphous ribbon of this composition and attributed the second peak to the ordering of the off-stoichiometric equilibrium Fe_3Si phase. The thermograms of the particles (Figure 5) show a range of crystallization behavior depending upon the particle size. The 20-30 μm particles crystallize at the lowest temperature for the particles with a small shoulder on the high temperature side of the peak. The <10 μm particles exhibit a sharp crystallization peak at about the temperature of the shoulder of the crystallization peak of the 20-30 μm particles. The 10-20 μm particles appear to have components of both the high and low temperature events. The temperature of the start of crystallization, T_x, and of the peak of heat evolution, T_p, increased with decreasing particle size. The values of T_x are plotted as a function of particle diameter and ribbon thickness in Figure 6. The 17 micron thick ribbon was cast at a higher wheel speed than was the 27.5 micron thick ribbon. There is no significant effect of ribbon thickness on T_x but there is a marked effect of particle diameter on T_x. Similar differences

also appear in the measurement of the heat of crystallization, ΔH, made in the DSC using the heat of fusion of In as the standard. Values of ΔH for the particles are plotted in Figure 7. Included in the plot are values of ΔH for the first crystallization peak of the ribbon (R1) and ΔH for all three exothermic peaks (R2). The presence of multiple peaks in the DSC test of the ribbon makes it difficult to compare directly with the powders. However, in the case of the particles, there is a marked decrease in the heat of crystallization with increasing size.

3.3 Transmission Electron Microscopy

3.3.1 Crystallization of Ribbon

Samples of ribbon and powders were examined by transmission electron microscopy. All samples were thinned by ion milling. Figure 8 shows a TEM of a sample of as-cast ribbon. The electron diffraction pattern of this area is shown in the inset. The diffuse nature of the diffraction rings indicate the amorphous nature of the ribbon. The d-values of the ribbon are listed in Table I.

Approximately 5 mg samples of ribbon were crystallized by heating in the DSC at 40 K/min to the desired temperature at which point the samples were rapidly cooled. Figure 9a shows crystals in a sample of ribbon heated to 832 K, the temperature at which crystallization just begins. The electron diffraction pattern of the crystal indicated by the arrow is shown in Figure 9b. The pattern reveals both a highly perfect single crystal and the amorphous rings of the matrix. The crystal is Fe_3Si with a $<3\bar{2}1>$ normal. There are also present crystals of different morphology, an example of which is shown in Figure 10a. The electron diffraction pattern (Figure 10b) of the crystal indicated by the arrow in Figure 10a shows it to be alpha iron. Thus, both Fe_3Si and alpha iron occur as initial crystallization products in the ribbon.

Other samples of ribbon were heated to 890 K and rapidly cooled in the DSC. This temperature includes all of the exothermic events for the ribbon. It is assumed that all of the crystallization and transformation events have been completed. Figure 11 shows an area of ribbon given this anneal. There is no amorphous material remaining. The grain size averages about 0.05 micron and it is difficult to distinguish one grain from another. Analysis of the diffraction pattern of this area, (inset, Figure 11), shows the presence of both Fe_2B and Fe_3Si grains. Additional samples of ribbon were annealed at higher temperatures for longer times to increase the grain size to the point where selected area diffraction patterns could be obtained from individual grains. Figure 12 shows an area of ribbon which was annealed for 1 hr at 973 K in nitrogen. The grain size has increased by a factor of two as a result of the anneal. However, as the electron diffraction pattern of this area in Figure 12 (inset) shows, the grain size is still too small for crystal structure determination by selected area diffraction of individual crystals. Another ribbon sample was heated at 1073 K for 24 hrs in nitrogen. As Figure 13 shows, there has been considerable grain growth during this anneal and grains of both phases are clearly delineated. The electron diffraction pattern, Figure 13b, obtained from the grain containing the stacking faults (marked #1) shows this grain to be b.c.t. Fe_2B. The crystallographic normal of this grain is $<\bar{5}13>$. The diffraction pattern of the speckled grain adjacent to the faulted grain in Figure 13a (marked #2) is shown in Figure 13c. This grain is orthorhombic $Fe_3(Si,B)$ with a $<513>$ normal and $a_0 = 5.35$, $b_0 = 6.66$, and $c_0 = 4.47$ A.

3.3.2 Crystallization of 10-20 Micron Diameter Particles

Samples of 10-20 micron diameter powder were heated to 843 K in the DSC. According to the thermograms, this is the temperature at which crystallization is just beginning in the 5 mg sample. The number of crystals in the particles ranged from none to the number observed in the particle shown in Figure 14. These crystals are also the largest ones found in this sample, ranging from about 400 to about 800 A in diameter. The most representative distribution of crystals in this sample is similar to that shown in Figure 15a, a region in another particle of this sample. The diffraction pattern of the crystal marked by the arrow in Figure 15a is shown in Figure 15b. This crystal has the b.c.t. Fe_3B structure[13] as do all of the crystals formed in the early stage of crystallization of the 10-20 micron powder. As discussed elsewhere[4] and observed in Figure 14, some of the spark eroded particles contain small (90 to 500 A diameter) voids. It appears, from examination of Figure 14, that the Fe_3B crystals may favor nucleation at the voids.

3.3.3 Crystallization of 20-30 Micron Diameter Particles

Samples of 20-30 micron powder were heated to 857 K, the temperature for the beginning of crystallization for powders of this size, and quickly cooled. The area shown in Figure 16a contained the largest number of crystals and the largest crystals of this sample. Most of the areas contained few or no crystals. It would appear that most, if not all, of the crystals nucleated at voids in this area and the void-nucleated crystals appear to be much larger than those that formed in regions free of voids. Each crystal appears

to be formed of subcrystals growing independently of adjacent subcrystals. Dark field transmission electron microscopy caused only the subcrystals to be in contrast, not the entire crystal. The subcrystals consist of fine striae about 3.5 to 4 nm thick. Electron diffraction patterns of the crystals indicated by the arrows in Figure 16a, Figure 16b, show these crystals also to be b.c. tetragonal Fe_3B.

Another sample of the 20-30 micron powder was heated to 50% of crystallization in the DSC. In this sample, some particles had not begun to crystallize whereas other particles were completely crystallized. Selected area diffraction of the crystallized particles showed both $Fe_3(Si,B)$ crystals and Fe_2B crystals. Other samples of this powder were heated to 925 K, a temperature well above that for complete crystallization in the DSC. An example of the microstructure is shown in Figure 17. The morphologies of the crystals are quite different from those of the crystals in the ribbon heated to complete crystallization (see Figure 11). Nevertheless, electron diffraction (inset, Figure 17) shows the crystals to be Fe_2B, Fe_3Si, and $Fe_3(Si,B)$ just as in the completely crystallized ribbon. Again, to differentiate among the grains, additional samples of the 20-30 micron powder were heated at 1073 K for 8 hrs to increase the grain size. The resulting microstructure was very like that of the ribbon given the same heat treatment in that the annealed powder particles consisted of well defined relatively large grains of faulted Fe_2B and speckled $Fe_3(Si,B)$ or Fe_3Si.

4. DISCUSSION

4.1 Long-Term Anneals

The long-term low-temperature anneals increase the average hyperfine field, H_{mean} of the particles while H_{mean} of the ribbon is essentially unchanged by the anneal (see Table II). According to previous arguments,[3] an increase in H_{mean} indicates a decrease in the metalloid concentration about the Fe sites. In essence, the chemical short range order (CSRO) of the particles is increased by the low temperature anneal. The ribbon, already having a greater degree of CSRO is unchanged by the anneal. Even after the long time anneal, the extent of CSRO in the particles is still less than that of the ribbon. The few alpha-iron crystals that are formed in the ribbon as a result of the 648 K anneal might be expected for an alloy with less than 20 atom percent boron.[7] The lack of crystallization in the particles in the 648 K anneal may be attributed to the greater degree of chemical disorder in the particles compared with that of the ribbon; that is, the activation energy for diffusion may be higher in the particles.

4.2 Crystallization

The initial formation of alpha-iron crystals and Fe_3Si or $Fe_3(Si,B)$ crystals in the ribbon rapidly heated to just the beginning of crystallization in the DSC would be expected for an iron-base alloy with a low concentration of boron.[7,8] This assumes that silicon acts as a substitutional element replacing Fe atoms to at least 15 atom percent. Thus, the alloy is hypoeutectic with respect to boron and alpha iron crystals should be expected to form early in crystallization. Silicon makes it easier to make the alloy amorphous by liquid quenching than would be the case for the $Fe_{75}B_{25}$ alloy. This is because the silicon sharply increases the crystallization temperature[14] and, presumably the glass transition temperature, while at the same time decreasing the melting temperature.[15] This should provide a greater glass forming tendency for the $Fe_{79}Si_{15}B_{10}$ alloy compared with the $Fe_{75}B_{25}$ alloy which is more stable than the alloys of Fe with less than 17 atom percent boron.[16] The chemical disorder is greater in the more rapidly quenched particles than it is in the less rapidly quenched ribbon. Thus, there is a greater probability for some iron atoms in the particles to have a greater number of boron atoms as neighbors compared with the ribbon. It appears that the boron enrichment is sufficiently great to form Fe-B "clusters"[16,17] which act as nuclei for the formation and growth of Fe_3B crystals in the particles. These nonequilibrium crystals are also formed in both the hypoeutectic[7] and the hypereutectic[13] Fe-B alloys.

When the ribbon is heated to complete crystallization in the DSC, the equilibrium phases for this alloy, Fe_2B and Fe_3Si, are present[8,19] as is the $Fe_3(Si,B)$ phase. The last phase does not appear in the chill cast crystalline alloy.[20,21] The Fe_2B phase occurs as faulted crystals and the cubic Fe_3Si or the orthorhombic $Fe_3(Si,B)$ phases appear as distinct speckled crystals (for instance, see Figure 11). These crystals do not change their morphology when heated for 24 hrs at 1073 K to effect grain growth. The completely crystallized 20-30 μm powders also consist of the Fe_2B, Fe_3Si, and $Fe_3(Si,B)$ phases but the microstructure is markedly different from that of the ribbon. It appears that the particles arrive at the same high temperature phases by a different route than is the case for the ribbon. That is, the ribbon transforms directly to the Fe_2B, Fe_3Si, and $Fe_3(Si,B)$ phases while the particles first form Fe_3B which, at higher temperatures, transforms to alpha iron and Fe_2B while the Fe_3Si and $Fe_3(Si,B)$ grains are forming. This is what the microstructure in Figure 17 would indicate. Even so, after 24 hrs at 1073 K, the powder particles consist of faulted Fe_2B grains and speckled Fe_3Si and $Fe_3(Si,B)$ grains.

The activation of crystallization is more difficult in particles than in the ribbon. This is consistent with reduced CSRO in the particles compared with the ribbon since more diffusion would be required for nucleation and growth of the equilibrium phases in the particles. The greater degree of order in the ribbon would be more likely to provide for the growth of the equilibrium or near-equilibrium phases Fe, Fe_3Si, and $Fe_3(Si,B)$ in the early stages of crystallization.

5. SUMMARY AND CONCLUSIONS

Amorphous ribbons and powders of the alloy $Fe_{75}Si_{15}B_{10}$ (atom percent) were prepared by chill casting and by spark erosion, respectively. Crystallization characteristics of both forms of the amorphous alloy were measured by differential scanning calorimetry, X-ray diffraction, and transmission electron microscopy. The crystallization temperature, T_x, of the largest particles was higher than that of the ribbon. Both T_x and the heat of crystallization increased with decreasing particle size. The DSC thermograms also showed marked differences from ribbon to particles and with decreasing particle size.

The first crystals to form on heating the ribbon were the stable phases alpha iron and Fe_3Si. At higher temperatures Fe_2B and $Fe_3(Si,B)$ crystals appeared along with the Fe_3Si crystals as the final crystallization product. On the other hand, the first crystals to form in the powder were the metastable b.c. tetragonal Fe_3B. At higher temperatures Fe_3Si, $Fe_3(Si,B)$, and Fe_2B crystals formed. Previous work has shown that the particles are more chemically disordered than the ribbon leading to the conclusion that there is a greater probability for the iron atoms in the particles to have more boron atoms as neighbors compared with the ribbon. These Fe-B "clusters" in the particles act as nuclei for formation and growth of the nonequilibrium Fe_3B crystals in the particles. Subsequent transformation of the Fe_3B at higher temperatures produces the final crystallization product of Fe_2B, Fe_3Si, and $Fe_3(Si,B)$.

ACKNOWLEDGEMENTS

The ribbons were prepared by W.R. Rollins. The spark erosion runs were carried out by E.S. Shaver, Jr. under the supervision of E. Matthews. Scanning microscopy was done by the members of the Microchemical and Surface Analysis Unit and the X-ray diffraction and optical microscopy was done by members of the X-ray and Microstructural Analysis Unit. The Mössbauer measurements were made by K.F. Wall. A.L. Ortiz, Jr. made the magnetic measurements and N.A. Marrota the DSC measurements. The authors are grateful for discussions with B. Cantor of Oxford University and with J.D. Livingston. This work was supported in part by the Office of Naval Research.

REFERENCES

1. T. Yamaguchi and K. Narita, *IEEE Trans. Magn. 13* (1977) 1621
2. A.E. Berkowitz and J.L. Walter, *Rapid Solidification Processing Principles and Technologies II,* Claitor's Publishing Division, Baton Rouge, LA (1980) 294.
3. A.E. Berkowitz, J.L. Walter, and K.F. Wall, *Phys. Rev. Letters 46* (1981) 1484.
4. A.E. Berkowitz and J.L. Walter, *Materials Sci. and Eng. 55* (1982) 275.
5. J.L. Walter, *Rapidly Quenched Metals, III, Vol. 1,* The Metals Society, London (1978) 30.
6. E.F. Koch and J.L. Walter, *Proceedings 39th Meeting of Electron Mic. Soc. of America,* Claitor's Publishing Div., Baton Rouge, LA (1981) 144.
7. J.L. Walter, S.F. Bartram, and I. Mella, *Materials Sci. and Eng. 36* (1978) 193.
8. T. Masumoto, H. Kimura, A. Inoue, and Y. Waseda, *Materials Sci. and Eng. 23* (1976) 141.
9. A. Inoue, T. Masumoto, M. Kikuchi, and T. Minemura, "1685th Report of the Research Institute for Iron, Steel and Other Metals" (1979) 127.
10. H. Fugita, K. Hashimoto, and T. Tabata, *Materials Sci. and Eng. 45* (1980) 221.
11. R. Window, *J. Phys. E4* (1971) 401.
12. T. Kemeny, I. Vincze, H.A. Davies, I.W. Donald, and A. Lovas, *Proc. Budapest Conf. on Metallic Glasses, 1980,* Kultura (P.O. Box 149, Budapest, Hungary, H-1389) 239.
13. J.L. Walter, S.F. Bartram, and R.R. Russell, *Met. Trans. A 9A* (1978) 803.
14. H.N. Ok, K.S. Balk, and C.S. Kim, *Phys. Rev. B, 24* (1981) 6600.
15. J.L. Walter, *Materials Sci. and Eng. 50* (1981) 137.
16. J.L. Walter, *J. of Non-Cryst. Solids 44* (1981) 195.
17. R. Oshima and F. Fujita, *Jap. J. of Appl. Phys. 12* (1981) 1.
18. I. Vincze, D.S. Boudreaux, and M. Tegze, *Phys. Rev. B 19* (1979) 4896.
19. T. Kemeny, I. Vincze, B. Fogarassy, and S. Arajs, *Phys. Rev. B 20* (1979) 476.
20. J.D. Livingston, A.E. Berkowitz, and J.L. Walter, *IEEE Trans. of Magnetics Mag 15* (1979) 1295.
21. A.E. Berkowitz, J.D. Livingston, B.D. Nathan, and J.L. Walter, *J. Appl. Phys. 50* (1979) 1754.

Figure 1 Scanning electron micrograph of amorphous spark eroded particles.

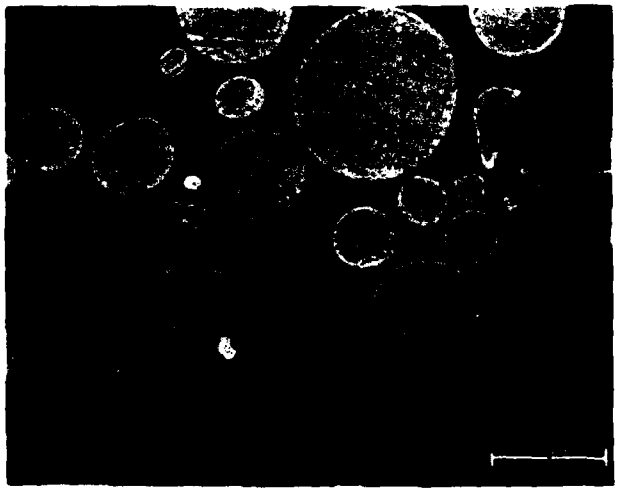

Figure 2 Optical micrograph of etched sections of unscreened particles.

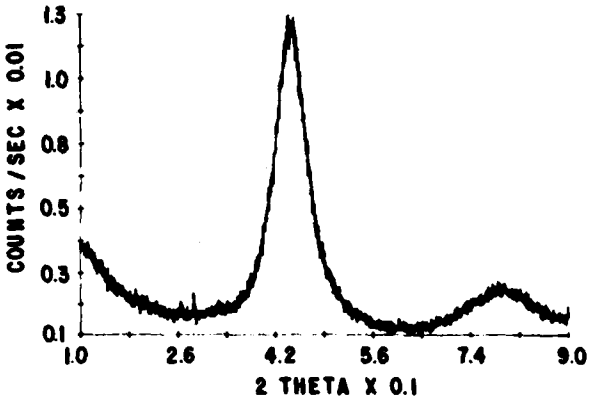

Figure 3(a) X-ray diffractometer trace of particles $<38\ \mu m$.

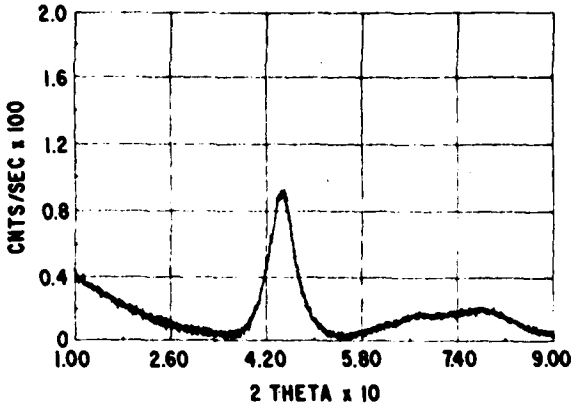

Figure 3(b) X-ray diffractometer trace of 27 μm ribbon.

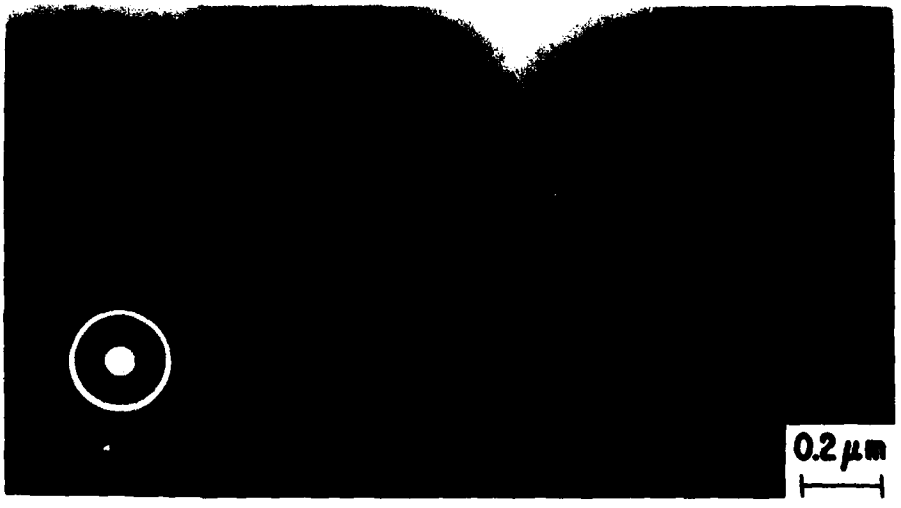

Figure 4 TEM and electron diffraction pattern (inset) of particle of 20-30 μm powder heated 21 days at 648 K.

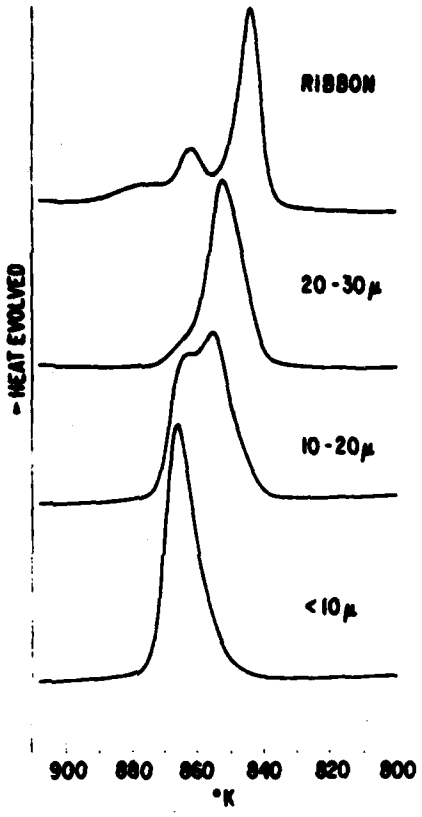

Figure 5 DSC thermograms of ribbon and powder of various size fractions. Heating rate 40°C/min.

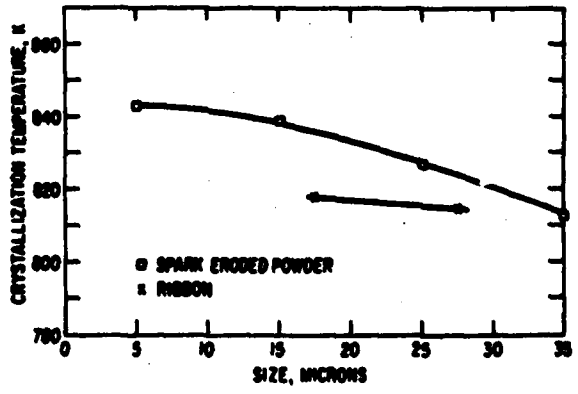

Figure 6 Crystallization temperature as a function of average particle diameter and ribbon thickness.

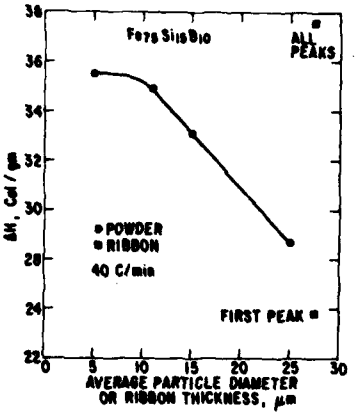

Figure 7 Heat of crystallization of particles and of ribbon as a function of diameter and thickness.

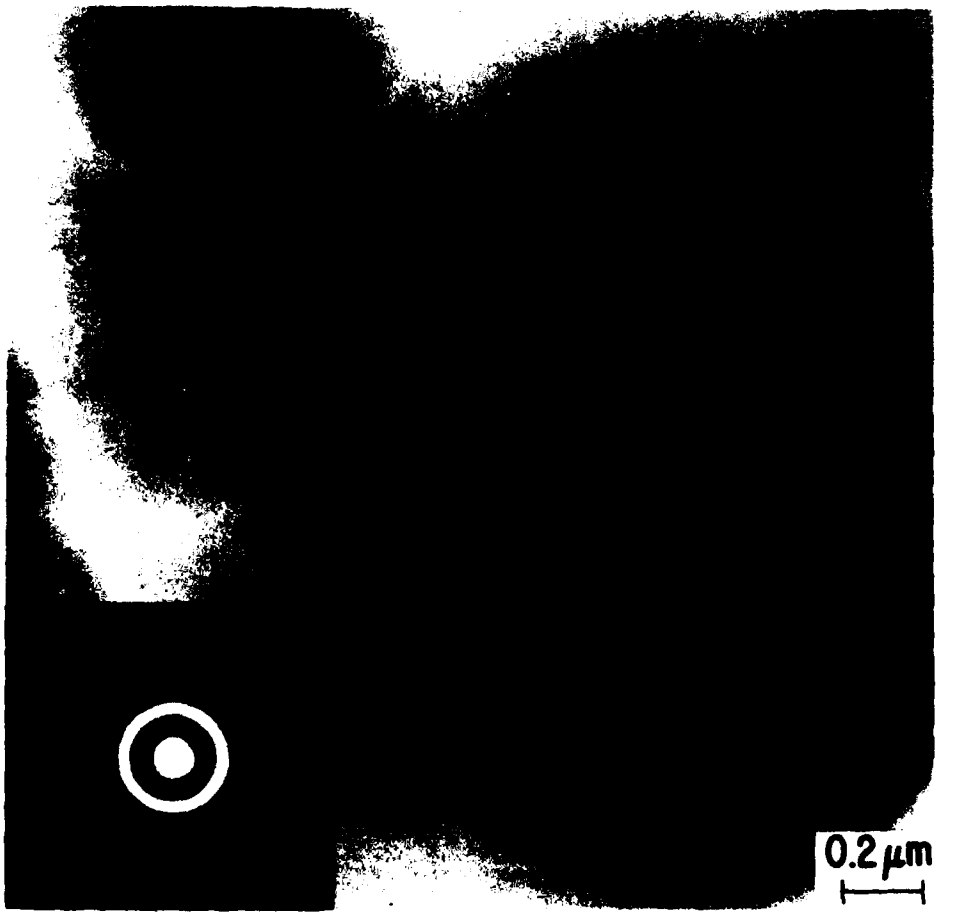

Figure 8 Transmission electron micrograph and electron diffraction pattern (inset) of as-cast ribbon.

Figure 9(a) TEM of ribbon heated to 832 K in DSC.

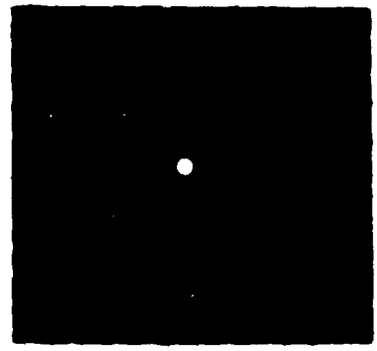

Figure 9(b) Diffraction pattern of Fe_3Si crystal indicated by arrow in Figure 9a.

Figure 10(a) TEM of ribbon heated to 832 K in DSC.

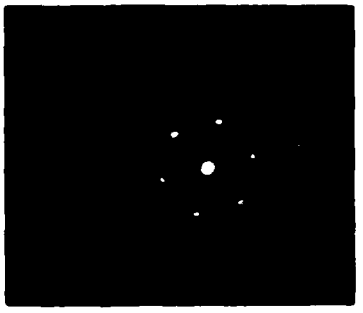

Figure 10(b) Diffraction pattern of α-Fe crystal indicated by arrow in Figure 10(a).

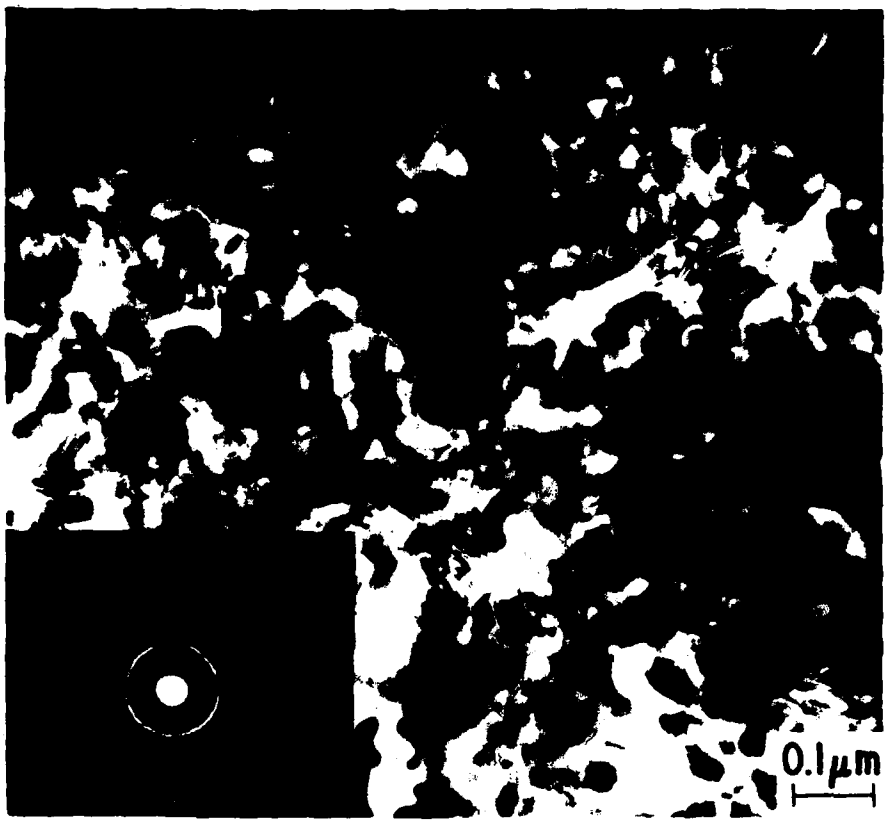

Figure 11 TEM of ribbon heated to 890 K in DSC. Diffraction pattern of area (inset).

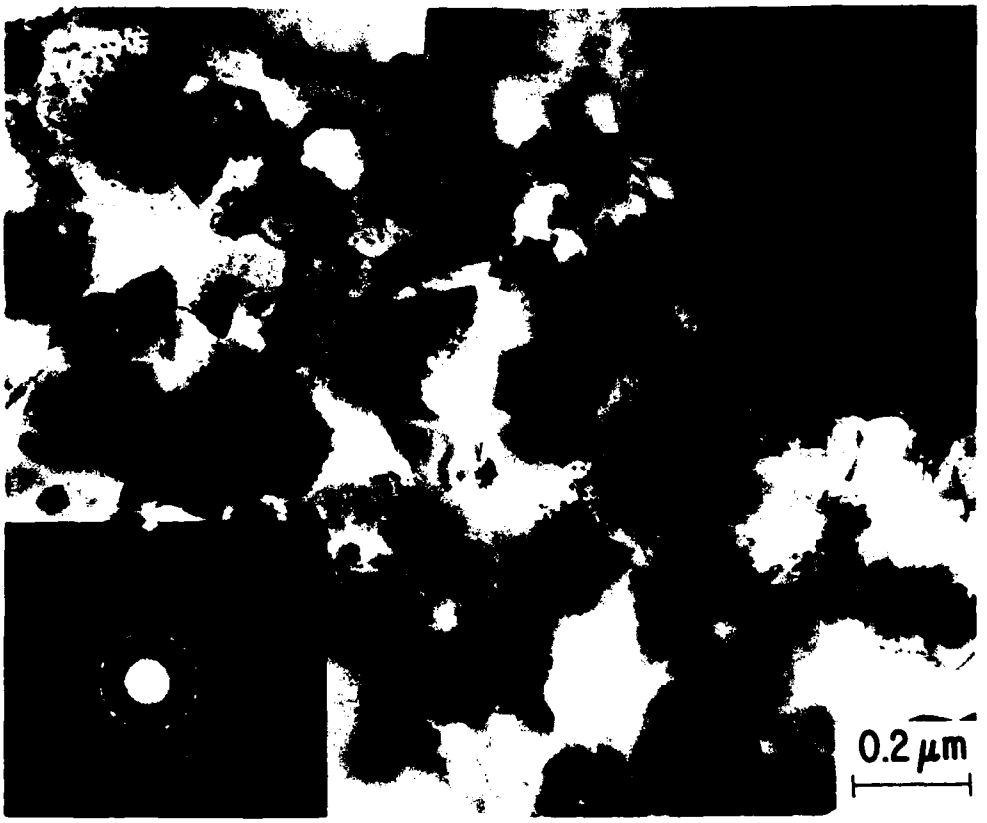

Figure 12 **TEM and diffraction pattern (inset) of ribbon heated for 1 hr at 973 K in N.**

Figure 13(a) TEM of ribbon heated for 24 hrs at 1073 K in N.

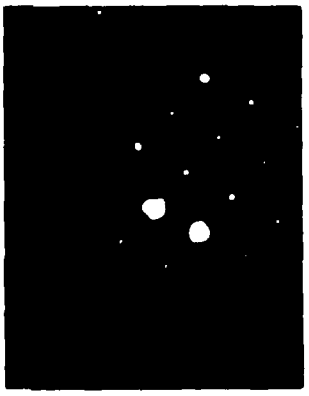

Figure 13(b) Diffraction pattern of crystal with fault (#1) in Figure 13a.

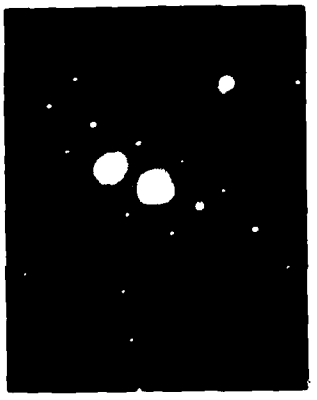

Figure 13(c) Diffraction pattern of speckled crystal (#2) in Figure 13a.

Figure 14 TEM of particle of 10-20 μm powder heated to 843 K in DSC.

Figure 15(a) ***Crystals in another particle of*** **10-20 μm powder heated to 843 K.**

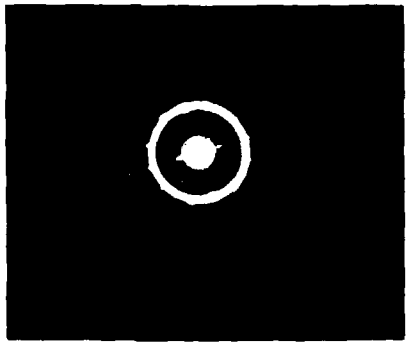

Figure 15(b) Diffraction pattern of crystal marked by arrow in Figure 15a.

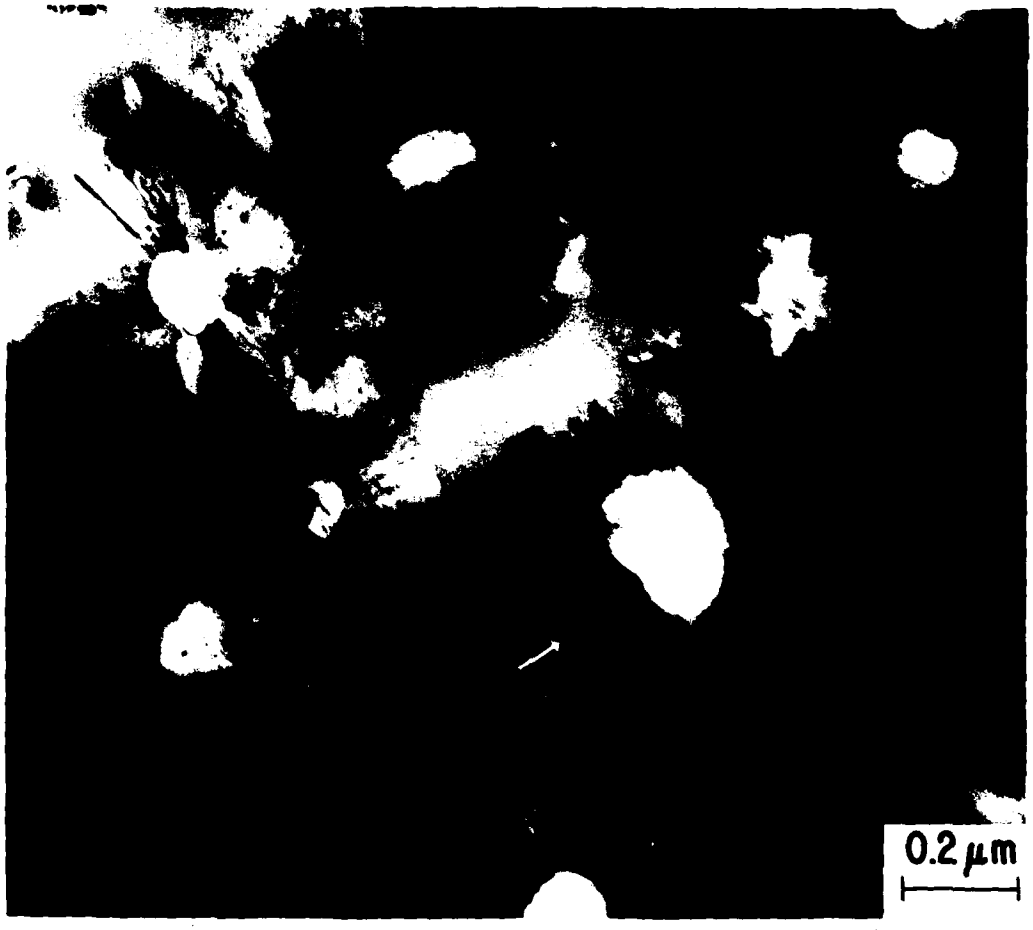

Figure 16(a) Crystals in 20-30 μm powder heated to 857 K.

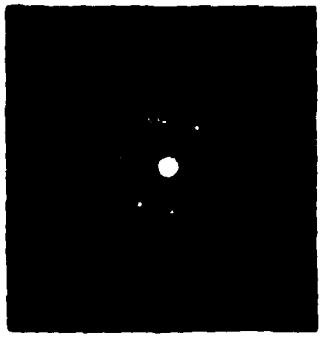

Figure 16(b) Diffraction pattern of crystal in Figure 16(a).

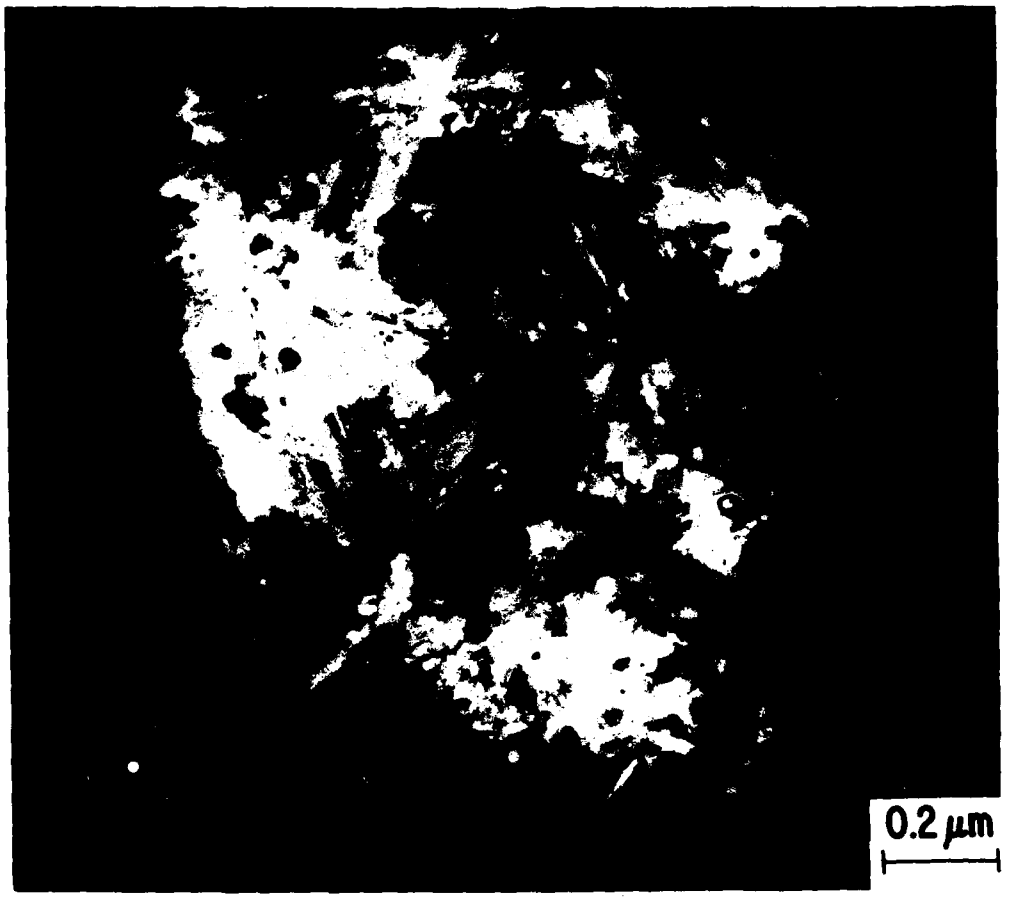

Figure 17 20-30 μ powder heated to 925 K to complete crystallization. Diffraction pattern of area (inset).

END

DATE
FILMED

6-83

DTIC